JGR Solid Earth

RESEARCH ARTICLE
10.1029/2020JB020448

Does Deep Tectonic Tremor Occur in the Central-Eastern Mediterranean Basin?

G. M. Bocchini[1], P. Martínez-Garzón[2], R. M. Harrington[1], and M. Bohnhoff[2,3]

[1]Faculty of Geosciences, Institute of Geology, Mineralogy and Geophysics, Ruhr University of Bochum, Bochum, Germany, [2]Helmholtz Centre Potsdam GFZ German Research Centre for Geosciences, Section 4.2 Geomechanics and Scientific Drilling, Potsdam, Germany, [3]Department of Earth Sciences, Institute of Geological Sciences, Freie University of Berlin, Berlin, Germany

Key Points:

- There is no unambiguous evidence for the occurrence of deep tectonic tremor in the central-eastern Mediterranean basin
- The thermal structure of subduction zones has an important control on deep tremorgenic conditions
- Very special physical conditions are required for deep tremorgenesis in settings that are not warm subduction zones

Supporting Information:

- Supporting Information S1

Correspondence to:
G. M. Bocchini,
gian.bocchini@rub.de

Citation:
Bocchini, G. M., Martínez-Garzón, P., Harrington, R. M., & Bohnhoff, M. (2021). Does deep tectonic tremor occur in the central-eastern Mediterranean basin? *Journal of Geophysical Research: Solid Earth*, *126*, 2020JB020448. https://doi.org/10.1029/2020JB020448

Received 22 JUN 2020
Accepted 3 DEC 2020

Abstract Tectonic tremor has been observed at the roots of many fault systems around the Pacific rim, including convergent and transform plate boundaries. The extent to which deep tremor signals are prevalent along fault systems elsewhere, including the Mediterranean basin, has not yet been documented in detail. A body of evidence suggests that tremor triggered during the surface waves of teleseismic events may commonly occur where ambient tremor during episodic tremor and slip episodes occur, suggesting triggered tremor provides a useful tool to identify regions with ambient tremor. We perform a systematic search of triggered tremor associated with large teleseismic events between 2010 and 2020 at four major fault systems within the central-eastern Mediterranean basin, namely the Hellenic and Calabrian subduction zones, and the North Anatolian and Kefalonia transform faults. In addition, we search for ambient tremor during a slow slip event in the eastern Sea of Marmara along a secondary branch of the North Anatolian Fault, and two slow slip events beneath western Peloponnese (Hellenic Subduction Zone). We find no unambiguous evidence for deep triggered tremor, nor ambient tremor. The absence of triggered tremor at the Hellenic and Calabrian subduction zones supports an interpretation of less favorable conditions for tremorgenesis in the presence of old and cold slabs. The absence of tremor along the transform faults may be due to an absence of the conditions commonly promoting tremorgenesis in such settings, including high-fluid pressures and low-differential stresses between the down-dip limit of the seismogenic layer and the continental Moho.

Plain Language Summary The discovery of slow earthquakes, or events with rupture velocities intermediate between traditional earthquakes and plate convergence rates, has revolutionized our understanding of the modes of stress release during the seismic cycle, and has implications for seismic hazard assessment. Here, we focus on a specific group of slow, low-amplitude earthquakes with energy concentrated in the 2–8 Hz frequency range that accommodate slip on faults where rock deformation transitions from brittle to plastic, namely tectonic tremor. To date, tectonic tremor is best documented primarily in fault systems along the Pacific rim. Whether the absence (or infrequent occurrence) of tremor outside of the Pacific rim is due to a sampling bias or due to non favorable physical conditions is still poorly understood. We perform a systematic search of deep tectonic tremor along four major fault systems in the central-eastern Mediterranean basin, where an unambiguous case is yet to be reported. We find no unambiguous evidence for deep tectonic tremor and conclude that very special conditions, such as anomalously high fluid pore pressures, significant frictional heating, etc., are required for tremorgenesis in settings that are not warm subduction zones, where deep tremor is abundant.

1. Introduction

The enhancement of geodetic and seismological monitoring systems over the last 2 decades has led to the discovery of various types of slow, transient deformation, also known as slow earthquakes. Slow earthquakes exhibit rupture velocities intermediate between those of traditional earthquakes and plate convergence rates (Obara, 2002; Obara & Kato, 2016; Rogers & Dragert, 2003) and may or may not radiate seismic energy (Obara & Kato, 2016; Peng & Gomberg, 2010). Tectonic tremor (hereafter referred to as tremor) belongs to the slow earthquake family and is defined as a long duration (up to minutes) and low-amplitude seismic signal with energy often concentrated between frequencies of 2–8 Hz (Obara, 2002). The occurrence of tremor, mostly composed of bursts of low frequency earthquakes (LFEs) (Shelly et al., 2007b), is usually

accompanied by short-term slow slip events (SSEs) (i.e., durations from days to weeks) and very low frequency earthquakes (VLFEs) (Obara & Kato, 2016). The coupled manifestation of tremor and short-term SSEs was first discovered in the Cascadia Subduction Zone (Rogers & Dragert, 2003) and has been termed episodic tremor and slip (ETS), where LFEs as large as M_w 2.6 have been reported during ETS in Cascadia (Bostock et al., 2015). Tremor occurring during ETS episodes is also referred to as spontaneous or ambient tremor.

Tremor episodes commonly occur in subduction zones slightly below the down-dip limit of the seismogenic zone at depths spanning the intersection of the down-going slab and the upper-plate Moho (Brown et al., 2009; Ghosh et al., 2009b; Ide, 2012; Obara, 2002; Wech & Creager, 2008), and mostly outline the upper boundary of continental Moho at the transform boundaries at which they have been observed (Horstmann et al., 2013; Nadeau & Dolenc, 2005; Shelly, 2017). Documented cases of tremor show that it also occurs up-dip or within the seismogenic zone (e.g., Costa Rica, Walter et al., 2011, 2013; NE Japan trench, Nishikawa et al., 2019). We therefore refer to tremor located below the down-dip limit of the seismogenic zone in the following as deep tremor.

Although the underlining physical mechanisms remain enigmatic, it is commonly accepted that slow earthquakes, including tremor, may straddle a transitional physical state between conditions favoring stick-slip behavior and stable sliding (Audet & Kim, 2016). It also appears that fault thermal structure affects the depth distribution and occurrence of deep tremor (Ide, 2012; Gao & Wang, 2017; Yabe et al., 2014) due to the primary temperature control on the brittle-plastic transition (Scholz, 1998). Numerical models suggest the occurrence of the brittle-plastic transition at depths shallower than the upper-plate Moho as essential condition for slow earthquakes, including deep tremor, occurrence in subduction zones (Gao & Wang, 2017). In fact, tremor has been primarily observed at young, warm subduction zones (Brown et al., 2009; Ide, 2012; Obara, 2002; Wech & Creager, 2008) where the brittle-plastic transition and peak dehydration reactions occur at shallower depths than in cold subduction zones (Peacock & Wang, 1999). The often observed patchy nature of the spatial deep tremor distribution (Ghosh et al., 2009b; Ide, 2012) indicates that its occurrence is also affected by other mechanisms, such as pore fluid pressure (Audet et al., 2009; Kodaira et al., 2004), rock frictional properties (Houston, 2015), fault geometrical complexities (Romanet et al., 2018), seafloor irregularities, and properties of the overriding plate (Nishikawa et al., 2019). Seismological investigations often reveal the presence of near-lithostatic pore fluid pressures in regions where deep tremor does occur (Audet et al., 2009; Audet & Kim, 2016; Kodaira et al., 2004). Recent studies that image the build-up and release of fluid pressures (i.e., fault-valve behavior) during ETS in Cascadia (Gosselin et al., 2020) and SSEs at the Hikurangi trench in New Zealand (Warren-Smith et al., 2019) support the relevant role of elevated pore fluid pressures in the genesis of slow earthquakes. Low effective stresses due to high fluid pressure is also the mechanism proposed to control tremor generation up-dip of the interplate seismogenic zone in subduction zones (Saffer & Wallace, 2015). Hence, potentially tremorgenic conditions could exist along many faults and possibly at different depths.

Another factor supporting the role of elevated pore fluid pressures in tremorgenic faulting conditions are the small stress perturbations that can trigger tremor. For example, peak ground velocities (PGV) as low as 0.01–0.03 cm/s generated from remote earthquakes, corresponding to dynamic stresses of about 1–3 kPa have been observed to trigger tremor (Chao et al., 2012a; Miyazawa & Brodsky, 2008; Peng et al., 2009), as have tidally induced stress changes on the order of ∼1 kPa (Rubinstein et al., 2008; Shelly et al., 2007a). While triggering thresholds appear to vary from region to region (Peng & Gomberg, 2010) and may be a function of station coverage and background tremor activity (Chao et al., 2012a), triggered tremor largely seems to occur in regions where ambient tremor is also generated (Figure 1; e.g., Chao et al., 2012a, 2012b, 2013; Fry et al., 2011; Ghosh et al., 2009a; Gomberg et al., 2008; Miyazawa & Brodsky, 2008; Miyazawa et al., 2008; Peng & Chao, 2008). As triggered tremor typically has larger amplitudes than ambient tremor (Rubinstein et al., 2007), a systematic search for triggered tremor provides a useful tool to identify regions that might also experience (undocumented) ambient tremor.

Despite the growing observations of both deep ambient and triggered tremor, one of the most striking features of all well-documented cases (i.e., visible at least at three seismic stations), is that they are primarily confined to transform and convergent plate boundary fault systems along the Pacific rim (Figure 1). To date, the Oriente Fault near Guantanamo Bay (Cuba) represents the only exception, with triggered tremor

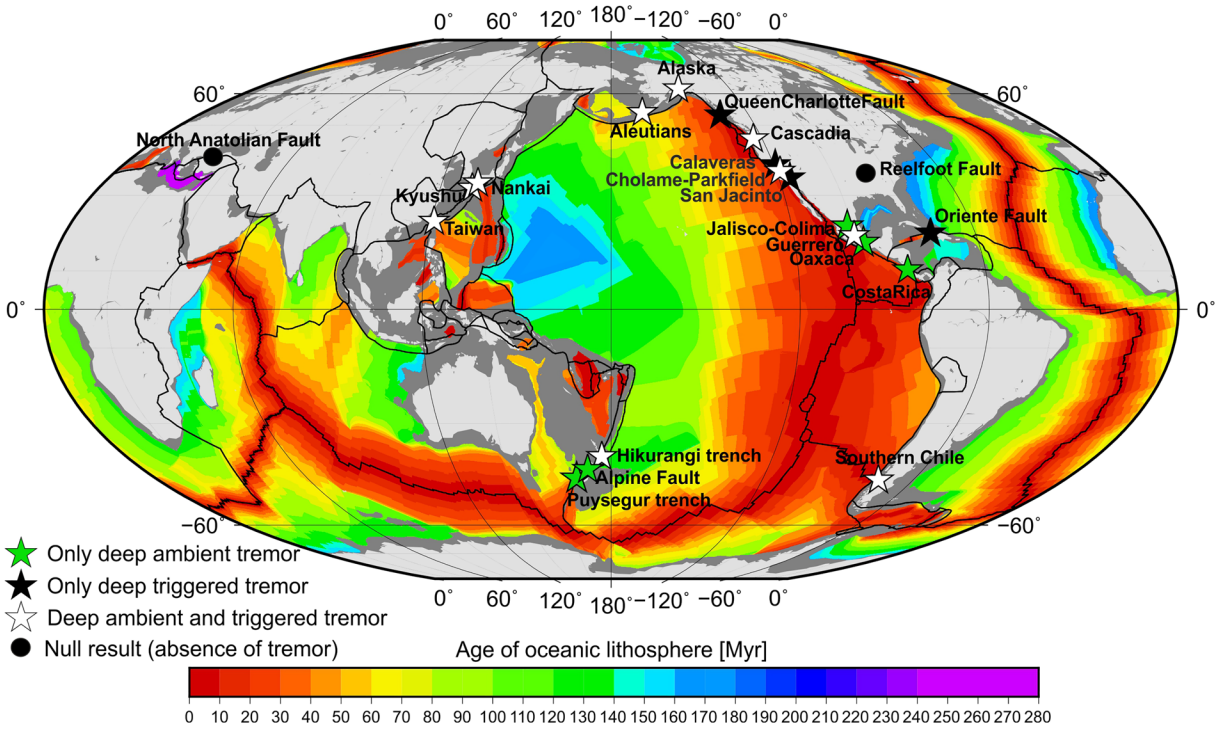

Figure 1. Global distribution of well-documented (observed at a minimum of three stations) sources of deep triggered and ambient tremor, which is confined primarily to the Pacific rim (Aiken et al., 2013; Brown et al., 2009, 2013; Brudzinski et al., 2016; Chao et al., 2012a, 2013; Chao & Obara, 2016; Ide, 2012; Kim et al., 2011; Nadeau & Dolenc, 2005; Peng et al., 2009; Romanet & Ide, 2019; Sun et al., 2015; Wech et al., 2012). Null results from Bockholt et al. (2014) and Pfohl et al. (2015). Oceanic lithosphere is colored according to age (Müller et al., 2008).

recorded at more than three stations during the surface wave shaking generated by two teleseismic events (Peng et al., 2013). (We omitted cases in which triggered tremor was recorded by a single station from Figure 1 due to the non constrainable hypocentral locations [deep or shallow] and the potentially ambiguous nature of the signals.) Whether the absence (or infrequent occurrence) of deep tremor outside of the Pacific rim is due to a sampling bias or to non favorable physical conditions is still poorly understood. The dearth of studies reporting null results, that is an absence of tectonic tremor (Bockholt et al., 2014; Pfohl et al., 2015; Yang & Peng, 2013; Figure 1) make it hard to address such a question.

In this study, we perform a systematic search of deep triggered tremor within the central-eastern Mediterranean basin with a focus on transform and subduction fault systems (Figure 2). We focus on the Hellenic and Calabrian subduction zones, and the Kefalonia and the North Anatolian transform faults (Figures 2a–2d) in our analysis, where no unambiguous example of ambient and triggered tremor has been reported to date. The four regions are ideal candidate study areas, as there is sufficient seismic station coverage over the past 10 years to detect deep triggered tremor, should it have occurred (Figures 2a–d, S1a and S1b). Furthermore, they are well-suited to explore physical factors that may favor or inhibit deep tremor occurrence for several reasons, including: (a) the presence of the oldest subducting lithosphere on Earth (Müller et al., 2008) and thicker and wider accretionary wedges compared to subduction zones in the Pacific rim (Clift & Vannucchi, 2004); and (b) the younger age and smaller accumulated displacement of transform faults (Şengör et al., 2005; van Hinsbergen et al., 2006) with respect to the Alpine and San Andreas transform faults (Dickinson & Wernicke, 1997; Norris & Cooper, 2001) (Figure 1). We also investigate the occurrence of ambient tremor during a SSE in the eastern Marmara Sea (Martínez-Garzón et al., 2019), along the North Anatolian Fault, and two SSEs beneath Peloponnese, in the western segment of the Hellenic Subduction Zone (Mouslopoulou et al., 2020).

Section 2 provides a tectonic overview of the study regions, followed by a description of the datasets and methods in Section 3. We report the results in Section 4 and discuss the implications of our study, including the similarities and differences with other fault systems in Section 5, and follow with conclusive remarks in Section 6.

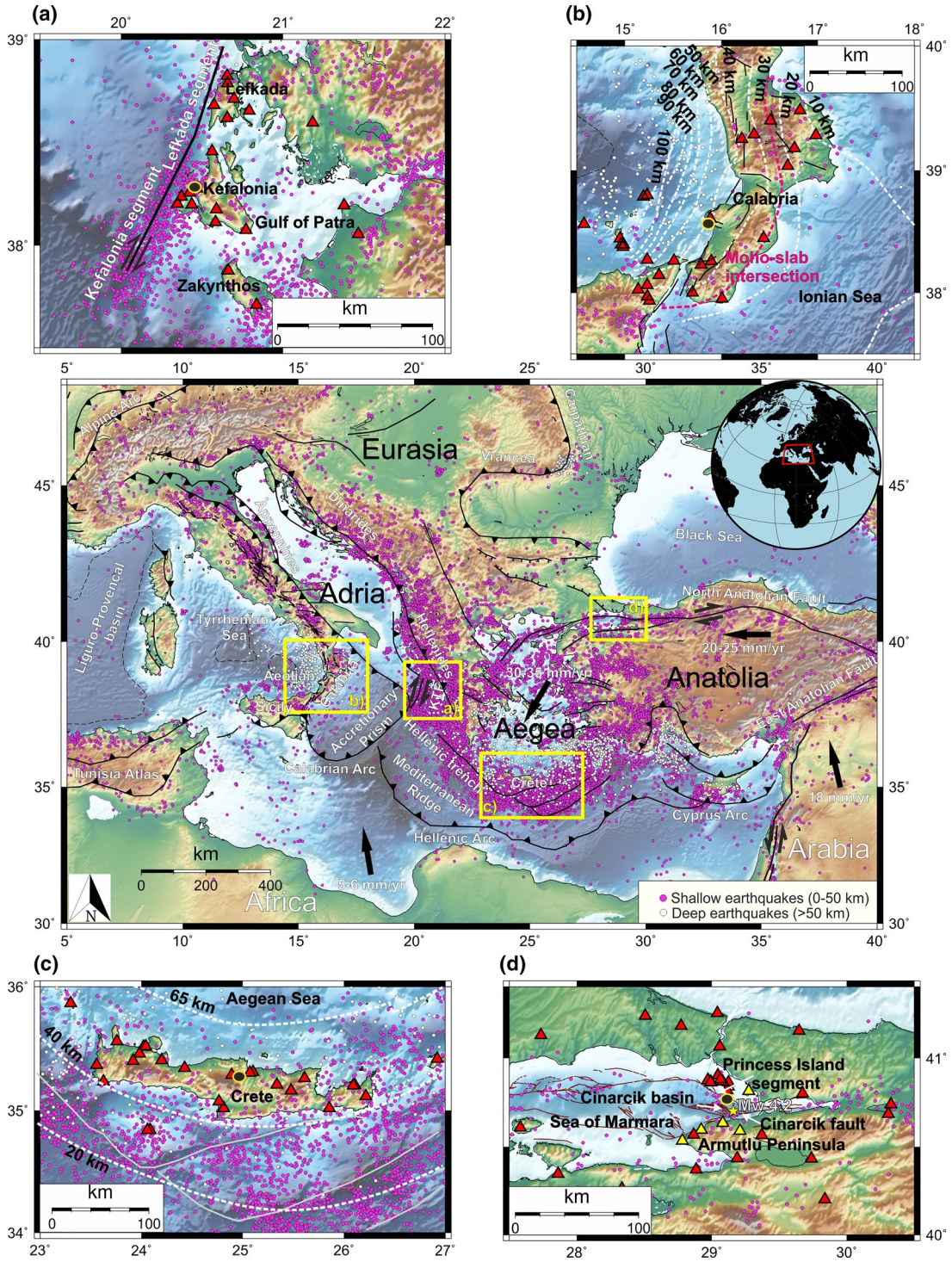

Figure 2. Main panel: Central and eastern Mediterranean region. Main tectonic elements (black lines) from Faccenna et al. (2014). Black arrows indicate the relative plate-microplate motion with respect to stable Eurasia (McClusky et al., 2000). We plot with purple (depth 0–50 km) and white (depth ≥50 km) dots all M ≥ 4 earthquakes documented by the International Seismological Centre (ISC) between 1964 and 2010 (ISC, 2020). Yellow boxes in the main panel indicate the four study regions: (a) Kefalonia Transform Fault, (b) Calabrian Subduction Zone; (c) Hellenic Subduction Zone, Crete; and (d) North Anatolian Fault, eastern Marmara Sea. Red triangles indicate seismic stations in the period 2010–2020 (not necessarily available in all investigated periods). Yellow triangles in panel d indicate borehole stations. Dashed white lines in panels (b and c) represent the top of the slab isodepths from Maesano et al. (2017) and Bocchini et al. (2018), respectively. Dashed magenta line in (b) indicates the location of the intersection with the overriding plate Moho. Yellow star in panel (d) indicates the epicentral location of the M_w 4.2 Yalova earthquake on June 25, 2016. Black circles with yellow edges indicate the location where initial Peak Ground Velocity values were estimated (Section 3). Bathymetry is from Ryan et al. (2009).

2. Plate Boundaries and Fault Systems in the Central-Eastern Mediterranean

The current Mediterranean basin tectonic setting arose from a complex interaction between the comparatively slow convergence of the African and Eurasian plates since the Cretaceous (Faccenna et al., 2014). Deformation concentrates along irregular, diffuse boundaries between continental and oceanic lithospheric fragments moving independently from the overall convergent motion (Figure 2; Faccenna et al., 2014). Low-to-moderate and occasionally large ($M > 7$) magnitude earthquakes (Guidoboni & Comastri, 2005) concentrate along the plate and microplate boundaries (Figure 2) as inferred from historical and instrumental seismicity. The central-eastern Mediterranean basin releases larger seismic moment and displays larger strain rates (Martínez-Garzón et al., 2020) relative to the western portion.

Although the Hellenic Subduction Zone (Figure 2c), the Calabrian Subduction Zone (Figure 2b), the Kefalonia Transform Fault (Figure 2a), and the North Anatolian Fault (Figure 2d) formed in the broad tectonic context of Africa-Eurasia convergence, they developed at different times and present distinct seismotectonic settings (e.g., kinematics, seismic moment release, age). In the following we delineate the main seismotectonic and geological aspects most relevant to deep tremorgenic conditions for each region.

2.1. The Kefalonia Transform Fault

The Kefalonia Transform Fault (Figure 2a) marks the western termination of the Hellenic Subduction Zone (Bocchini et al., 2018; Louvari et al., 1999; Pérouse et al., 2012). It started to form in the late Miocene-early Pliocene and has accumulated most of its ~60 km displacement over the last ~4–5 Ma (van Hinsbergen et al., 2006). The fault accommodates ~2 cm/yr of differential convergence between oceanic subduction and continental collision taking place to the north and south, respectively (Pérouse et al., 2012). It is composed primarily of two active segments, namely the Kefalonia and the Lefkada segments (Figure 2a) and exhibits pure dextral or transpressional slip motion (Louvari et al., 1999) with frequent $M > 6$ earthquakes (Papazachos & Papazachou, 2003). The regional seismicity distribution suggests a seismogenic layer extending between 3 and 16 km (Papadimitriou et al., 2017), with a continental Moho at ~28 km (Sodoudi et al., 2006).

2.2. The Calabrian Subduction Zone

The Calabrian Subduction Zone (Figure 2b) forms a narrow, arcuate subduction interface in southern Italy. The subduction of ~220–230 Ma old oceanic crust (Speranza et al., 2012) began ~80 Ma ago (Faccenna et al., 2001), and continues along a ~150 km wide sector between the Isthmus of Catanzaro to the north and the Strait of Messina to the south (Figure 2b; Maesano et al., 2017). The incoming plate has a 5–6 km thick layer of sedimentary cover forming a large accretionary prism (de Voogd et al., 1992). The subduction convergence rate is < 5 mm/yr (Pérouse et al., 2012), and has documented intraslab seismicity down to ~450–500 km (Selvaggi & Chiarabba, 1995), as well as a depletion of shallow interplate seismicity offshore in the Ionian Sea. The very low interplate seismicity and the low strain rates in the forearc (~10–20 nanostrain/yr) led some authors to consider the subduction as inactive (e.g., Pérouse et al., 2012). However, a recent study interprets unambiguous geodetic signals consistent with elastic strain accumulation at the megathrust being released episodically seismically and/or more likely through aseismic slip transients (Carafa et al., 2018). The interpretation is consistent with the large historical earthquake data in Calabria (Carafa et al., 2018), and would support the occurrence of slow earthquakes.

2.3. The Hellenic Subduction Zone

The Hellenic Subduction Zone (Figure 2c) defines an approximately 1,000 km long arcuate interface bounded by the Kefalonia Transform Fault to the west and a tear in the slab beneath south-western Turkey to the east (Bocchini et al., 2018). Oceanic lithosphere of age >220–230 Ma to the west (Speranza et al., 2012), and likely >300 Ma to the east (Granot, 2016) subducts at a rate of ~35–40 mm/yr (McClusky et al., 2000). A wide ~250–300 km long and up to 10–12 km thick sediment layer forming the Mediterranean Ridge Accretionary Prism overlays the down-going oceanic lithosphere (e.g., Bohnhoff et al., 2001; Kopf et al., 2003). Nubi-

an-Aegea convergence generates intense seismicity with magnitudes exceeding M ≥ 4 (Figure 2), including earthquakes as large as M∼8 as reported in historical catalogs (Papazachos & Papazachou, 2003). Seismic and geodetic studies suggest that more than 70%–80% of the relative plate motion occurs asesimically (Becker & Meier, 2010; Saltogianni et al., 2020; Vernant et al., 2014). Very recently, Mouslopoulou et al. (2020) reported two SSEs beneath the western coast of Peloponnese south of Zakynthos (Figure S1b). Approximately two months of plate motion acceleration preceded both SSEs. Each geodetic transient related to the SSEs lasted for ∼5–6 months (i.e., September 24, 2014 to March 20, 2015 and May 14, 2018 to October 25, 2018) and likely occurred between 20 and 40 km depth along the plate interface (Mouslopoulou et al., 2020).

Crete represents a horst structure in the central Hellenic forearc (Figure 2c) currently undergoing fast uplift and extension (Meier et al., 2007). Subduction south of Crete started about 20–15 Ma, when the plate boundary stepped back to the southern edge of an accreted microcontinent, building most of the present continental area (Thomson et al., 1999). The megathrust south of Crete exhibits intense microseismicity that abruptly terminates at ∼40 km depth below the southern coastline of the island (Meier et al., 2004), where the upper-plate crustal thickness is ∼30–35 km (Bohnhoff et al., 2001; Meier et al., 2007).

2.4. The North Anatolian Fault

The North Anatolian Fault is a 1,200-km-long right-lateral transform fault forming the boundary between the Eurasian Plate and the Anatolian microplate with relative displacement of ∼20–25 mm/yr (Figure 2d; McClusky et al., 2000). Formation started 12–13 Ma ago during the late phase of Arabia-Eurasia collision that accumulated a maximum displacement of ∼85–90 km decreasing from east to west (Bohnhoff et al., 2016). The North Anatolian Fault generates intense seismicity and frequent M > 7 earthquakes (Bohnhoff et al., 2016), such as the earthquake sequence in the 20th century that ruptured all but the Sea of Marmara segments (Stein et al., 1997). The Sea of Marmara region (Figure 2d) makes up the western portion of the North Anatolian Fault, and is in a transtensional state that represents a pull-apart basin within two major branches of the North Anatolian Fault that are ∼100 km apart (Armijo et al., 2002). It formed as part of a NS-extensional regime related to the fast rollback of the Hellenic Subduction Zone with the strike-slip regime being active since ∼2.5 Ma (Le Pichón et al., 2016; Şengör et al., 2005). The northern part of the Sea of Marmara is characterized by the presence of three deep basins separated by bathymetric highs, from east to west: the Çınarcık, Central, and Tekirdag basins (Armijo et al., 2002). The Çınarcık Fault bounds the Çınarcık Basin to the south and the Princess Island Fault segment bounds it to the north (Figure 2d). Precise hypocentral solutions suggest a seismogenic layer extending down to 10–15 km in the eastern Sea of Marmara (Wollin et al., 2018) while the Moho is found at 26–41 km depth (Jenkins et al., 2020; Zor et al., 2006).

The analysis of recent, high temporal resolution, geodetic data revealed the existence of temporal fluctuations of the creep rate with detection of accelerating bursts of shallow (i.e., 0–5 km) creep events along the segments of the North Anatolian Fault that ruptured during the 1999 Izmit (Aslan et al., 2019) and the 1944 Ismetpasa earthquakes (Rousset et al., 2016). On June 25, 2016, a ∼50-daylong SSE was recorded along the Çınarcık Fault below the eastern Sea of Marmara, which was interpreted as the strain release equivalent of a M_w 5.8 at the depth of 9 km (Martínez-Garzón et al., 2019). The authors assume the source location to be near to the M_w 4.2 Yalova earthquake (Malin et al., 2018) that occurred during the onset of the SSE (Figure 2d), although the depth was difficult to constrain after being recorded at a single station.

A previous study found no evidence for triggered tremor and no unambiguous evidence for ambient tremor on the central segment of the North Anatolian Fault near Ismetpasa (Pfohl et al., 2015), while here we focus on the recently densely instrumented eastern Sea of Marmara (Figure 2d).

3. Data and Methods

In the description that follows, we restrict the analysis of triggered tremor in the Hellenic Subduction Zone to the segment south of Crete due to the high station-density and quality of open-access seismic data relative to adjacent arc segments. Similarly, the North Anatolian Fault analysis focuses on the eastern Sea of

Marmara due to the density of station coverage from local network deployments. We report in Table S1 a detailed list of the seismic networks, stations and instrument types used.

As a first criteria to search for deep triggered tremor, we identify prospective triggering teleseismic earthquakes by selecting all events from the International Seismological Centre (ISC) catalog (ISC, 2020) with $M_w \geq 6.5$, hypocentral depths ≤ 50 km, and epicentral distances ≥ 800 km that generated a theoretical PGV larger than 0.01 cm/s within each study region. We restrict our analysis to large and shallow potential triggering mainshocks, because they are most effective in generating large surface waves at teleseismic distances that have the greatest potential of triggering tremor. We calculate theoretical PGV values at a point in the middle of each study region (Figures 2a–2d) using a ground motion empirical relationship (Aki & Richards, 2002; Lay & Wallace, 1995):

$$M_s = \log A_{20} + 1.66 \log \Delta + 2.0 \quad (1)$$

$$\mathrm{PGV} \approx 2\pi A_{20} / T \quad (2)$$

where M_s is the surface wave magnitude, A_{20} is the amplitude (in microns) of the Airy phase (surface wave with a 20 s period), Δ is the source-receiver (epicentral) distance, and T is the surface wave period (20 s). We assume $M_s = M_w$ as first approximation, as M_s generally saturates at higher magnitudes than the threshold cutoff. We download all mainshock candidate waveforms from the European Integrated Data Archive (EIDA, http://www.orfeus-eu.org/data/eida/, last accessed February 2020). In addition to publicly available data (AFAD, 1990; AUTH, 1981; GEOFON, 1993; INGV, 2006; KOERI, 2001; MedNet, 1990; NOA, 1997; TEIC, 2006; UA, 2008; UP, 2000), we use data from dense local deployments, namely the PIRES network (GFZ Potsdam BU-Kandilli, 2006) and the GONAF borehole network (Bohnhoff et al., 2017) to search for triggered tremor in the eastern Sea of Marmara.

As a second criteria for culling the list of candidate mainshocks, we calculate the observed PGV_{obs} value as the average value between the three components from all the available broad-band stations within each region (Figures 2a–2d), and reject events with average PGV_{obs} <0.01 cm/s (Figures 3a–3d). We retain a total of 16 candidates for the Hellenic and Calabrian subduction zones and for the Kefalonia Transform Fault and of 18 events for the North Anatolian Fault (Figures 3a–3d, Table S2). Table S2 provides a complete list of candidate mainshocks. Nearly all selected mainshocks are either strike-slip or reverse faulting earthquakes (Figures 3a–3d), and cover a wide range of back azimuths, with a gap to the south (Figures 3e–3h).

We manually search for cases of triggered tremor by visually inspecting waveforms surrounding the time interval predicted for the passage of surface waves in each region. We calculate theoretical surface wave arrivals using the TauP package (Crotwell et al., 1999) and the iasp91 velocity model (Kennett & Engdahl, 1991) in Obspy (Beyreuther et al., 2010), and search temporal windows starting when a phase traveling at 4.4 km/s (approximate Love wave arrival) reaches the station and terminating with the predicted arrival of a Rayleigh phase traveling at 2.0 km/s. The time window choice ensures that Love and Rayleigh waves with the highest triggering potential and amplitudes are included in the analysis. We rotate horizontal components to transverse and radial directions to visually confirm the correct arrival time of Love and Rayleigh waves, respectively. Following a well-established procedure, we search for non impulsive, coherent signals after applying either a 2–8 Hz bandpass filter or a 5 Hz highpass filter to remove the low-frequency teleseismic signal (i.e., primary and secondary arrivals) and preserve tremor signals in the frequency band where it is commonly observed to be most energetic. We require any prospective triggered tremor signal to be recorded by at least three seismic stations to ensure the signal is local and of tectonic origin. We also investigate low amplitude and long duration signals recorded only at two stations.

In addition to visual inspection, we also employ an envelope cross-correlation (Ide, 2010, 2012) to detect ambient tremor during the SSE in the eastern Sea of Marmara during an extended time period (from June 02, 2016 to July 30, 2016) encompassing the SSE documents in Martínez-Garzón et al. (2019) and the two geodetic transients, in 2014–2015 (from September 24, 2014 to March 20, 2015) and in 2018 (from May 14, 2018 to October 25, 2018), along the western segment of the Hellenic Subduction Zone (Mouslopoulou et al., 2020). The procedure entails creating daily envelopes of signals filtered between 2 and 8 Hz and

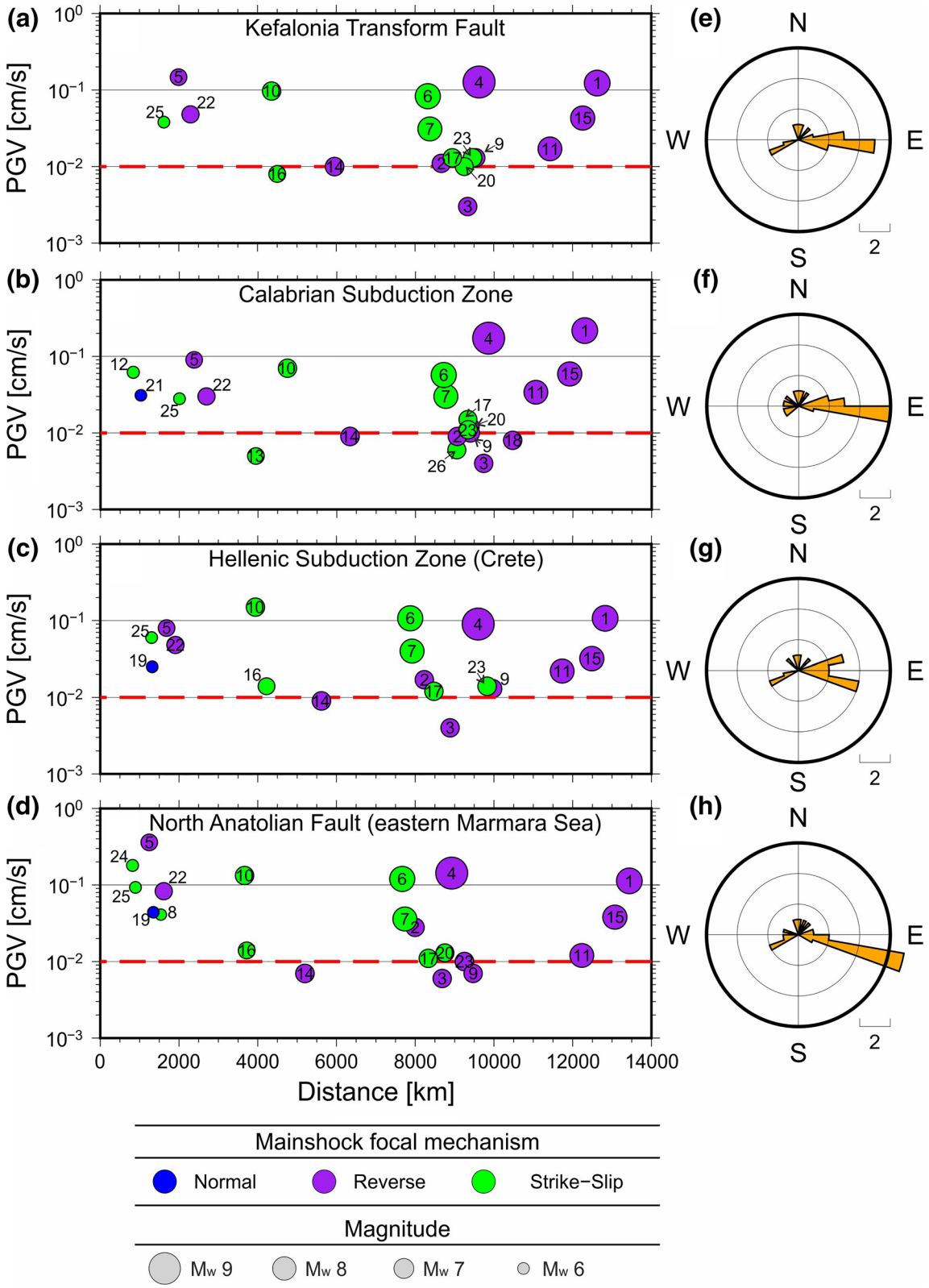

Figure 3. Candidate mainshocks around which the search for deep triggered tremor is centered with respective PGV values (a–d). (a–d) Symbol sizes correspond to magnitude, while color code corresponds to focal mechanism type. Dotted red lines indicate lower threshold of 0.01 cm/s Peak Ground Velocities (PGV) considered for mainshock candidates in this study. Observed PGV (PGV_{obs}) is calculated as the average value (unfiltered traces) among the three components of all the available broad-band stations within each region. (e–h) Back azimuths of candidate mainshocks producing $PGV_{obs} \geq 0.01$ cm/s. Numbers are event IDs and associated events are reported in Table S2.

cross-correlating horizontal channels at stations located < 100 km apart. An event is detected when a minimum cross-correlation value (0.5–0.7) is exceeded at a minimum number of channels (5–8). A more detailed description of the method is available at Ide (2010; 2012) and it is also provided in the supplement along with details on the station configuration (Text S1). To verify the efficacy of the automatic detection, we test its ability to detect several cataloged tremor signals near the Parkfield-Cholame segment of the San Andreas Fault, where tremor is widely documented (Horstmann et al., 2013; Nadeau & Dolenc, 2005; Shelly, 2017), using the same settings as for the eastern Sea of Marmara (Figure S2).

Finally, because we do not know a priori whether tremor occurs in any of the study regions, we perform synthetic tests to quantify the thresholds of detection in each of the regions. We generate synthetic tremor waveforms under realistic conditions using the Pyrocko toolbox (Heimann et al., 2017) based on the expected source locations, station coverage, and noise conditions in each region. In cases where no tremor is detected, the synthetic test allows us to quantify tremor detection thresholds so that we can quantify the minimum event size that would likely be observed. We provide a detailed description of the method in the supplement (Text S2).

4. Results

The manual inspection of waveforms during the passage of surface waves from events in Table S2 at seismic stations along four major fault systems within the central-eastern Mediterranean basin reveals no unambiguous case of triggered tremor at any of the study areas (Section 4.1), nor ambient tremor (Section 4.2) during the documented SSEs.

4.1. Triggered Tremor

We find no unambiguous evidence for triggered tremor beneath Crete, along the Hellenic Subduction Zone, beneath Calabria at the Calabrian Subduction Zone, at the Kefalonia Transform Fault, and in the eastern Sea of Marmara during the time period from 2010 to 2020. Although the minimum number of three stations may be a strict criterion relative to previous studies, we also observe no coherent tremor-like signals by reducing the minimum number of required stations to two. The waveforms after applying a bandpass filter in the frequency range 2–8 Hz show a distinct lack of tremor energy at a representative sample of stations during the surface wave shaking of the teleseismic mainshocks inducing some of the largest PGV_{obs} within each region (Figure 4). In addition, we show the expected amplitudes of deep synthetic tremor episodes (in blue) with respect to those of real waveforms (gray) filtered in the same frequency band (Figure 4). Overlaying the synthetic tremor waveforms provides an indication of the smallest tremor-like signals we would be able to detect within the surface wave shaking, should they have occurred. We plot the smallest magnitude bursts of LFEs that would be detectable at a minimum number of two or three stations.

We do observe potentially triggered LFEs at stations located along the Aeolian Arc, the volcanic arc of the Calabrian Subduction Zone (Figures 2b and S3). Two of the most striking signals are observed at station ILLI on Lipari Island (Figure S4) and at stations ISTR and IST3 on Stromboli (Figure S5). However, despite the good correlation between PGV_{obs} and low frequency signal occurrence, we cannot consider them as triggered signals. First, neither case fulfills the criterion of tremor-like signals exhibiting signal coherency at minimum three stations. In addition, careful inspection of the waveforms from one day before to one day after the mainshock reveals that the signal detected at station ILLI (Figure S4) is likely noise, due to the highly regular and repetitive nature of the candidate tremor signal (starting at ~6 a.m. and ending at ~5 p.m.) in the frequency band of interest (2–8 Hz and higher). The signal observed at stations ISTR and IST3 on Stromboli (Figure S5) is very likely a LFE of volcanic origin. However, we note that we also observe several LFEs both before and after the ground shaking induced by the teleseismic event. Moreover, the slab interface at the stations closest to where the tremor-like signal is observed is located at ~100 km depth beneath the volcanic Arc (Maesano et al., 2017). A seismic signal originating at 100 km depth would be inconsistent with an origin in the deep tremor zone, which is expected at corresponding to ~25 km depth at the observed location (Figure 2b). The synthetic tests suggest a detection threshold of M_w ~1.3–1.5 for bursts of LFEs at the Calabrian Subduction Zone (Figures 4b and 5a) based on LFEs that would nucleate at

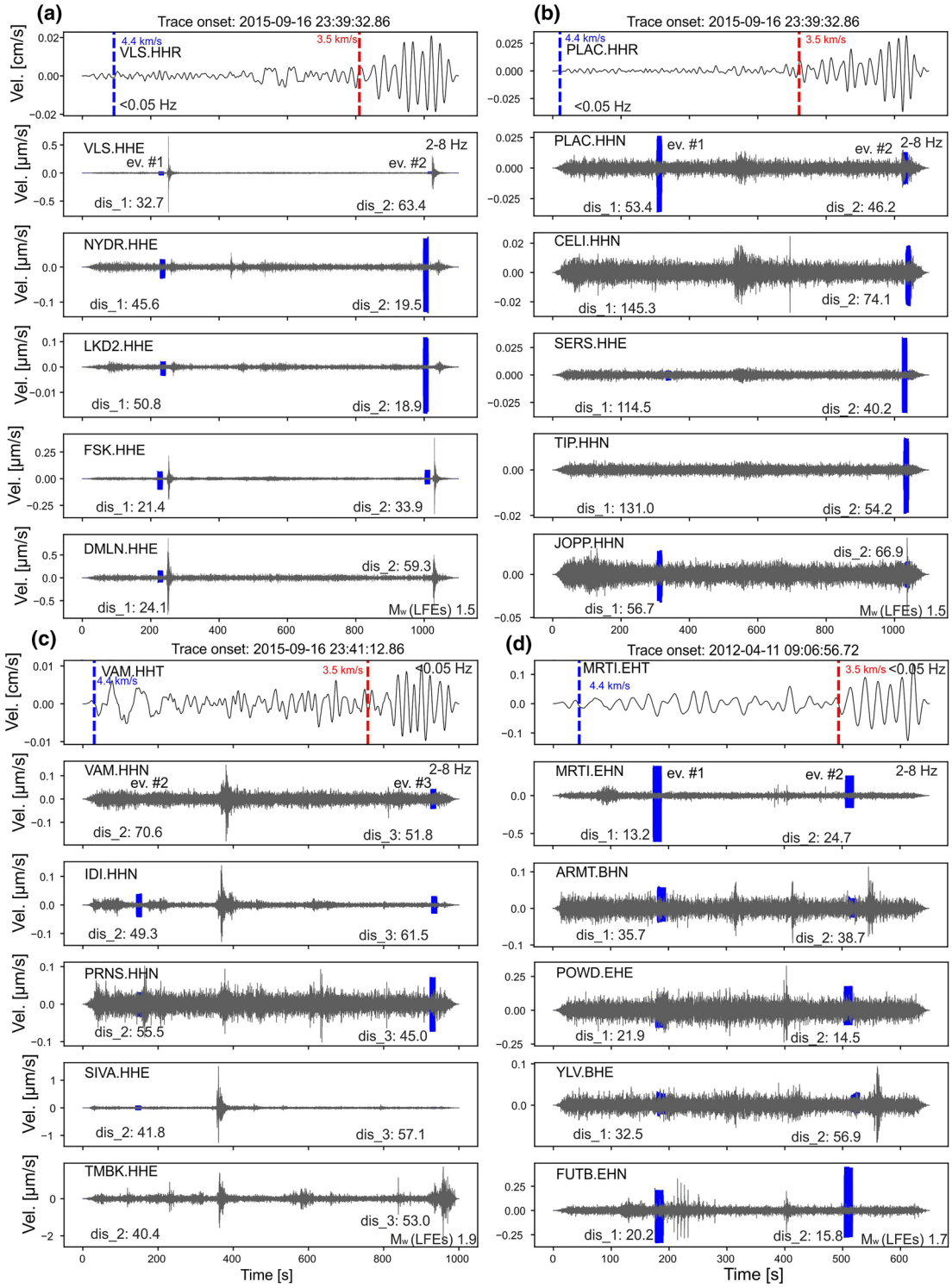

Figure 4. Example of waveforms exhibiting a lack of evidence for triggered tremor at the (a) Kefalonia Transform Fault, (b) Calabrian Subduction Zone, (c) Hellenic Subduction Zone (Crete) during the M_w 8.3 Illapel, Chile earthquake (ID 15 in Figure 3 and Table S2); and (d) North Anatolian Fault (Eastern Sea of Marmara) during the M_w 8.6 Sumatra, Indonesia earthquake (ID 6 in Figure 3 and Table S2). The dashed blue and red lines in the topmost panels indicate the estimated arrival time of phases traveling at 4.4 and 3.5 km/s, respectively, used as preliminary arrival time of Love and Rayleigh waves. Dark gray traces are the real waveforms filtered between 2 and 8 Hz, while blue traces show synthetic tremor waveforms. The bottom-right of each panel reports the M_w of individual LFEs in the synthetic tremor episodes. The location of the synthetic tremor events (ev. #1, ev. #2., ev. #3) and of seismic stations is shown in Figure S3. We report the source-receiver hypocentral distances in kilometer (dis_1, dis_2, dis_3, where the number refers to the event). A detailed view of synthetic tremor episodes is provided Figure S8. Waveforms in the topmost panels are low-pass filtered below 0.05 Hz, while the others are bandpass filtered between 2 and 8 Hz.

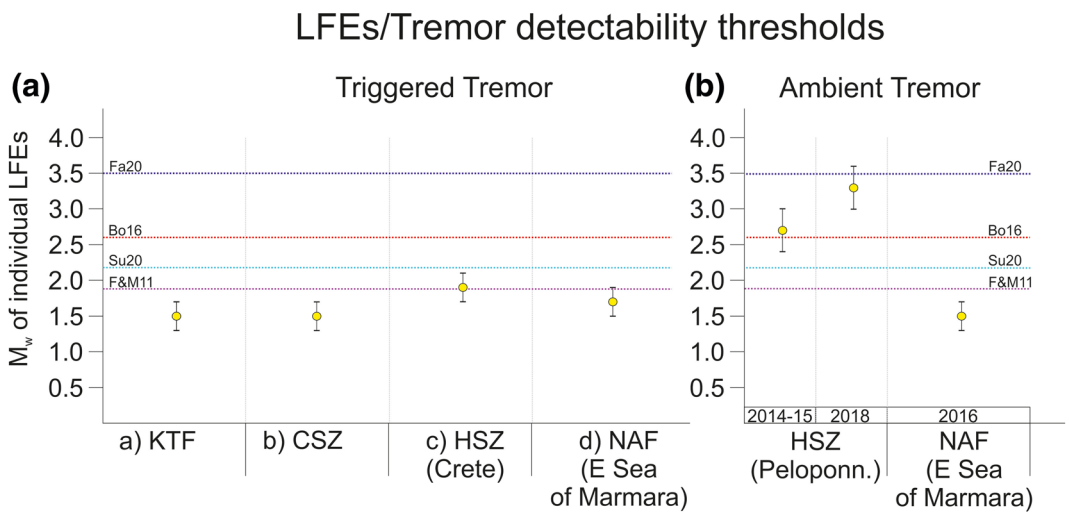

Figure 5. Estimated detectability thresholds for (a) triggered, and (b) ambient tremor episodes for each region analyzed in this study (Figures S1 and 2). M_w refers to values for individual Low Frequency Earthquakes (LFEs) comprising the tremor episodes. For reference, the dashed horizontal lines indicate the M_w of the largest detected LFEs within tremor episodes at several fault systems around the Pacific rim, including the Guerrero trench (Fa20, Farge et al., 2020), the Cascadia Subduction Zone (Bo15, Bostock et al., 2015), the San Andreas Fault (F&M11, Fletcher & McGarr, 2011) and the Nankai trench (Su20, Supino et al., 2020). CSZ, Calabrian Subduction Zone; HSZ, Hellenic Subduction Zone; KTF, Kefalonia Transform Fault; NAF, North Anatolian Fault. For more details on the synthetic tests performed to estimate the magnitude thresholds we refer the reader to Text S2.

26 km depth, namely around the intersection between the continental Moho and the subducting slab. We test epicentral locations in southern, central, and northern Calabria (Text S2, Figure S3b). The indicated magnitude threshold refers to the station configuration available from the 2011 onward. In 2010 the smaller number of available stations would prevent the observation of similar M_w ~1.3–1.5 LFEs at more than one or two stations.

The seismic stations on Crete exhibit evidence for a single tremor candidate during the M_w 8.3 Illapel (Chile) earthquake (ID 15 in Figure 3, Table S1). However, although visible at three or four stations (Figure S6) the signal is observed before the arrival of surface waves, when PGV_{obs} is smaller than 0.01 cm/s, suggesting an ambient, rather than triggered origin. We explore the possibility that the detected signal (Figure S6) could represent ambient tremor by running a matched-filter detection in EQcorrscan (Chamberlain et al., 2018). We used 6 and 8 second-long signal time windows, filtered between 2 and 8 Hz from both the horizontal channels of the three stations where the signal was clearly visible (i.e., TMBK, SIVA, and IDI; Figures S6 and S7; refer to supporting information Text S3 for additional details on matched-filter detection). We correlate the templates with continuous data in 1-day time windows before and after the tremor-like signal occurrence. Observations of ambient tremor in other fault zones rarely document isolated tremor events, but more commonly clustered, prolonged activity. The matched-filter detection yields traditional earthquake detections, some of which (e.g., at 18:23 and 19:00 on September 16, 2015) are reported in the revised catalog from the National Observatory of Athens (https://bbnet.gein.noa.gr/HL/databases/database, last accessed August 31, 2020). We observe that the moveout of tremor-like signals at the different stations is consistent with that of the detected earthquakes, suggesting a similar epicentral location (Figure S7). Thus, we interpret the observed signal as an earthquake with low SNR rather than tremor. We estimate through the synthetic tests a minimum detection magnitude of M_w ~1.7–1.9 (Figures 4c and 5), where synthetic sources are located at 40 km depth, namely at the down-dip limit of the seismogenic zone (Section 2.3), beneath eastern, central, and western Crete (Figure S3c). The proposed threshold refers to the station configuration available for the period 2014–2019 when most of the stations from the Technological Educational Institute of Crete (TEIC, 2006) were operational, in addition to those of the National Observatory of Athens (NOA, 1997). Should deep tremor have occurred earlier, we would be able to observe it only at specific

locations, namely close to well instrumented parts of Crete (e.g., between stations IDI and SIVA, beneath central Crete; and between stations ZKR, LAST, and NPS beneath eastern Crete; Figure S3c).

We do not observe any tremor-like signal at seismic stations along the Kefalonia Transform Fault. However, our detection yields possible dynamically triggered local earthquakes, as in other regions (Figure 4a), which will with investigate further in a follow-up study of remote dynamic earthquake triggering. The synthetic tests suggest a detection threshold of M_w ~1.3–1.5 (Figures 4a and 5a) for bursts of LFEs nucleating at 16 km depth (down-dip limit of the seismogenic zone, Section 2.1) along the Kefalonia and Lefkada segments of the Kefalonia Transform Fault (Figure S3a). Synthetic tests indicate that we would not be able to detect deep tremor triggered by the M_w 8.8 2010 Maule and the M_w 9.1 2011 Tohoku earthquakes, at more than one station, should it have occurred, due to the poor station coverage.

Finally, we do not observe unambiguous triggered tremor activity in the eastern Sea of Marmara. Observed correlated signals are either associated to local earthquakes or to instrument/cultural noise. We estimate a detection threshold of M_w ~1.5–1.7 for the smallest LFE bursts on at least two seismic stations (Figures 4d and 5a). We assume our synthetic tremor sources to be located at two distinct places along the Princess Island segment of the North Anatolian Fault (Figures 2d and S3d) at a depth of 12 km, namely at the down-dip limit of the seismogenic layer (Section 2.4). The detection threshold is valid for the period 2010–2018, when the PIRES stations were available (GFZ Potsdam BU-Kandilli, 2006). We do not test the case of a triggered tremor source located along the Çınarcık Fault segment, as we already do it in the synthetic tests for ambient tremor (Section 4.2, supporting information Text S2) and we expect similar results, at least starting from 2015, the time period when the GONAF borehole data became available (Bohnhoff et al., 2017).

Figure 5a synthesizes results of the synthetic tests carried out to quantify the detection thresholds of triggered tremor for each of the study regions. All the regions show similar or lower minimum detection thresholds with respect to the maximum magnitude of LFEs reported from several fault systems, where deep tremor has been well documented (Figure 5). We attribute an uncertainty to each value that is related to the magnitude steps considered in the synthetic tests (Text S2) that takes differences observed from the analysis of several teleseismic events into consideration. We refer the reader to the supplemental material for details of the synthetic test (Text S2).

4.2. Ambient Tremor

We find no unambiguous examples of LFE/tremor activity accompanying the SSEs in the eastern Marmara Sea nor beneath western Peloponnese. The result is consistent with the absence of triggered tremor along the investigated fault systems. It is also generally consistent with observations elsewhere showing that triggered tremor tends to occur in regions where also ambient tremor occurs (Figure 1).

In addition to local earthquakes with energetic signals both within the 2–8 Hz band and higher than 5 Hz, we do detect signals with dominant frequencies in the tectonic tremor frequency band (2–8 Hz, Figure 6). However, other factors suggest that the signals as shown in Figure 6, are not tectonic tremor. The signal in Figure 6a has a duration >15 s and frequency content <10 Hz at the closest station. However, the same signal more closely resembles a local earthquake rather than tremor (Figure S9) at stations exhibiting a higher Signal-to-Noise-Ratio (SNR) (e.g., DRO Figure 6a). We also detect signals (S-waves) from more distant earthquakes that could be misinterpreted as tremor if one restricted observation to stations located near SSEs sources where tremor activity would be expected (Figure 6b). For example, the signal shown in Figure 6b exhibits low frequency energy at stations on the Armutlu Peninsula (e.g., ARMT, KURT, YLV). However, it exhibits the typical character of an earthquake at stations located to the west of the Marmara Sea (e.g., KRBG, RKY). Because of the occurrence of several examples as those reported in Figure 6, we visually check all detections. Due to the longer cumulative duration of the two geodetic transients (~1-year long) in the Hellenic Subduction Zone, we checked all detected signals with duration longer than 15 s (through a preliminary investigation we observed that signals shorter than 15 s were mostly local earthquakes and in a very few cases noise). We note that the synthetic tests suggest higher magnitude detectability thresholds for tremor episodes at the Hellenic Subduction Zone during the 2014–2015 (M_w ~2.7, Figures 5b and S10)

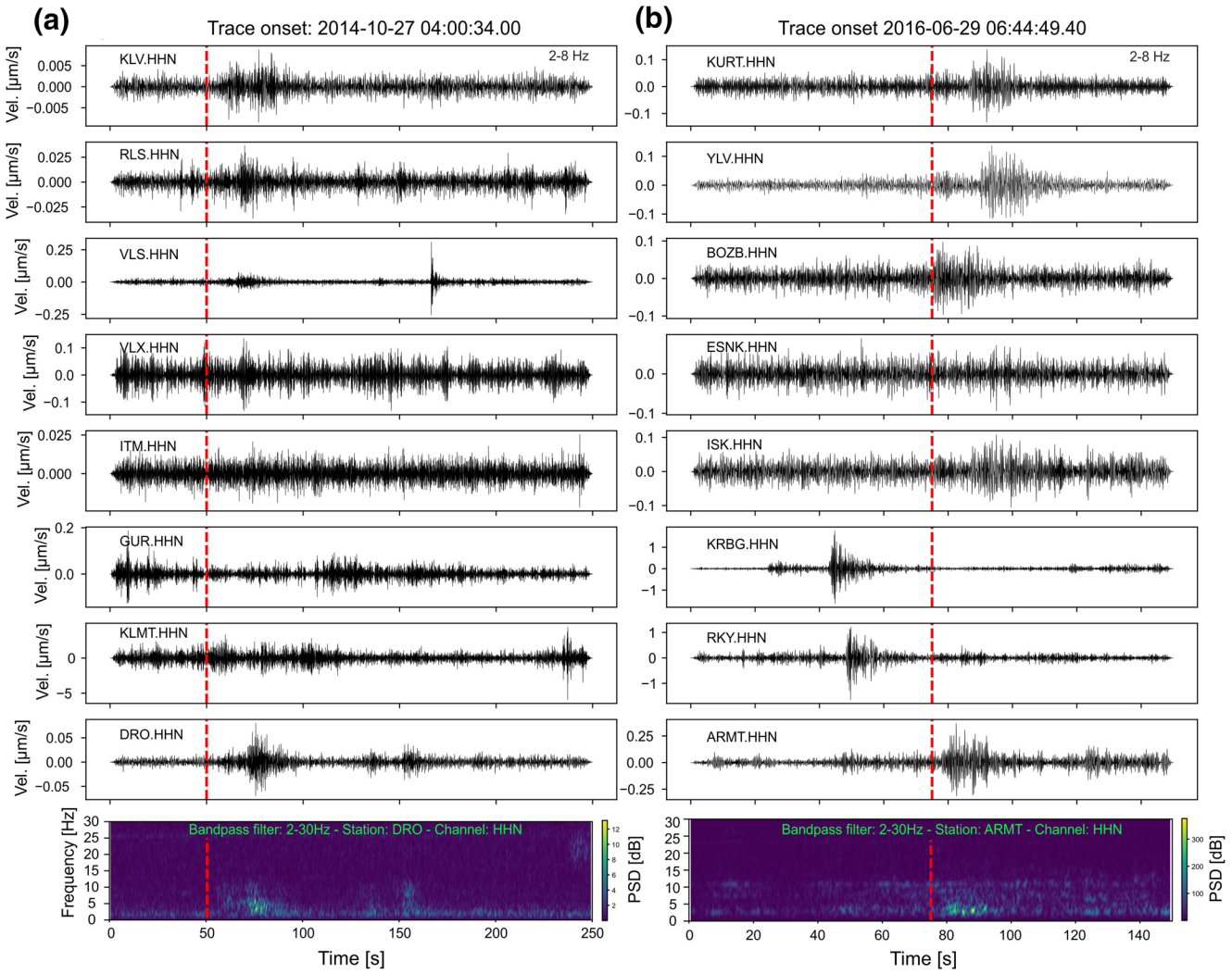

Figure 6. Example of detected signals using the automatic cross-correlation method at (a) the Hellenic Subduction Zone, and (b) in the eastern Marmara Sea along the North Anatolian Fault. The red line shows the detection time of the signal. The bottommost panels show the respective spectrograms of the signals shown in the panels above. The signals are detected by using half-overlapping windows of 300 s and a cross-correlation value of 0.6 at 5 or more channels at stations located <100 km apart on traces filtered between 2 and 8 Hz. Station location is shown in Figure S1. PSD, power spectral density.

and 2018 (M_w ~3.3, Figures 5b and S10) SSEs compared to the eastern Sea of Marmara (Figures 5b and S10) during the 2016 SSE (namely of ~M_w 1.5).

5. Discussion

The most prominent worldwide reported examples of ambient and triggered tremor are primarily limited to fault systems or plate boundary faults located along the Pacific rim (Figure 1), with the exception of the Oriente Fault in Cuba (Peng et al., 2013).

We note that the synthetic tests ensure that the absence of tremor in the Mediterranean basin is not related to the detectability thresholds of the employed networks in each region. The results indicate that in all the investigated regions but in Peloponnese (Hellenic Subduction Zone), we would be able to detect tremor episodes composed by LFEs of M_w larger than ~1.5–1.9 (Figure 5). Similar M_w LFEs or larger have been documented at several fault systems around the Pacific rim, including the Guerrero trench in Mexico (M_w 1.7–3 with a few events up to M_w 3.5, Farge et al., 2020), the Cascadia Subduction Zone (M_w 1.0–2.6,

Bostock et al., 2015), the Parkfield-Cholame segment of the San Andreas Fault (M_w 1.6–1.9, Fletcher & McGarr, 2011), and the Nankai trench in Japan (M_w 0.9–2.2, Supino et al., 2020). Previous studies have noticed lower M_w LFEs obtained from amplitude ratios with local earthquakes, which may underestimate LFE magnitudes due to differing frequency contents relative to local earthquakes (e.g., Bostock et al., 2015). We therefore report M_w values estimated from source parameter analysis and not those obtained by relative amplitude ratios. In the case of Peloponnese, during the SSE in 2014–2015 we would still be able to detect very vigorous tremor episodes composed by LFEs with similar M_w values to that of the largest recorded ones in Cascadia by Bostock et al. (2015) or at the Guerrero trench by Farge et al. (2020), while the network configuration and ambient noise level would have potentially missed tremor-like signals during the 2018 SSE. However, due the high similarity of the duration, location, and released seismic moment of the 2014–2015 and the 2018 SSEs (Mouslopoulou et al., 2020) it is possible that the absence of vigorous tremor episodes is common to both the SSEs.

One limitation of the triggered tremor analysis could be the short time period of investigation, particularly in cases where hypothetical deep tremor episodes would have inter-event periods longer than the 10 years investigated in this study. The relation between ambient and triggered tremor is still poorly understood (Chao et al., 2012a), however, many documented cases suggest that tremor is commonly triggered by low stress perturbations (e.g., Rubinstein et al., 2008; Shelly et al., 2007a) in areas where ambient tremor occurs, and the time windows considered should be ample to detect triggered tremor. For instance, along the Simi Valley segment of the San Andreas Fault in southern California, where no unambiguous case of ambient tremor is documented, apparent triggering thresholds are suggested to be much larger than those for the Parkfield–Cholame section of the San Andreas Fault (~>12 kPa and 2–3 kPa, respectively; Yang & Peng, 2013), where ambient tremor occurs. Another limitation could be the relatively low PGV_{obs} values recorded in our study regions with respect to circum-Pacific fault systems that lie closer to the sources of $M > 7$–7.5 earthquakes where tremor occurs. However, we note that the 0.1 cm/s threshold is exceeded during 4–5 events, or during three events when considering a 20 s period, within each region (Figures 3a–3d), and the estimated dynamic stresses perturbations are >9 kPa. Therefore, many of what appear to be the essential physical conditions associated with observed cases of triggering are met by the candidate mainshocks here. Thus, working on the assumption that the mainshocks generated sufficiently large stress perturbations to trigger tremor and that the seismic network coverage would be sufficient to detect them, in the following, we discuss similarities and differences between the Pacific and the Mediterranean regions and the possible causes of absence of deep tremor along the investigated subduction (Section 5.1) and transform fault systems (Section 5.2).

5.1. Absence of Tremor along the Calabrian and the Hellenic Arc

The most striking difference between the Pacific and the Mediterranean subduction zones is arguably the age of the down-going plate (Figure 1, Müller et al., 2008). In addition, the Mediterranean Sea is populated with wider and thicker accretionary prisms (Clift & Vannucchi, 2004), and convergence rates are on average lower within the Mediterranean basin (Matthews et al., 2016). All the above differences may be significant for tremorgenesis.

The age controlled thermal state of subducting slabs causes young slabs to dehydrate at shallower depths than older slabs, resulting in significant differences in subduction dynamics (Peacock & Wang, 1999). For instance, in warmer subduction zones (e.g., Cascadia, Mexico, Nankai), the brittle-plastic transition (assumed to be near the 350°C isotherm) occurs at shallower depths (Figures 7a and 7b; Peacock & Wang, 1999), and the mantle wedge corner is more hydrated (Abers et al., 2017) relative to older subduction zones (Figure 7). Thermal models for the Hellenic Subduction Zone show that the 350°C isotherm lies at ~60 km depth (Bocchini et al., 2018; Halpaap et al., 2019), well-below the down-dip limit of the seismogenic zone south of Crete and the intersection between the down-going plate and the upper-plate Moho (Figure 7b). Although the intersection between the upper-plate Moho and the down-going slab south of Crete is not well-defined, it is not located far from the southern coastline of the island (Bohnhoff et al., 2001). Hence, the absence of deep tremor is not surprising if we expect it to occur when the down-dip limit of the megathrust is shallower than the slab upper-plate Moho intersection depth

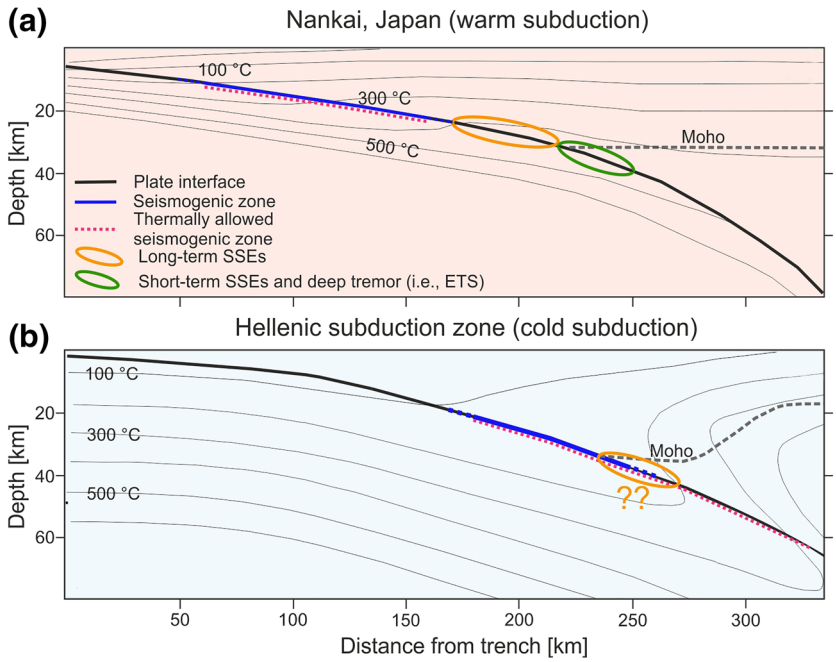

Figure 7. Sketch comparing typical slip behavior in a (a) warm subduction zone and a (b) cold subduction zone. (a) Cross-section along the Nankai trench (Japan) adapted from Gao and Wang (2017). (b) Cross-section across Crete using slab geometry and thermal structure from half-space cooling model in Bocchini et al. (2018). Upper-plate Moho depth in panel b is from Bohnhoff et al. (2001) and Meier et al. (2007).

(Figure 7a; Gao & Wang, 2017). A similar situation can be hypothesized for the Calabrian arc, due to the similar age of the subducting slab and its intersection with the upper-plate Moho at ~25 km. In fact, thermal models suggest that the 350°C isotherm occurs at depths much greater than 25 km (Syracuse et al., 2010). However, although not in oceanic crust as old as the Mediterranean oceanic lithosphere (>220–230 Ma), tremor does occur at subduction zones where the down-going slab is older than 100 Ma. Examples are the Hikurangi trench in New Zealand (Ide, 2012; Romanet & Ide, 2019) and the NE Japan Trench (Nishikawa et al., 2019), where both have common, unique conditions that may prime them for the occurrence of tremor. Deep tremorgenic conditions in New Zealand are explained to be consequence of the high frictional heating along the megathrust (Gao & Wang, 2017; Yabe et al., 2014) while in NE Japan, where tremor occurs at seismogenic depths, tremorgenic conditions are promoted by frictional heterogeneities likely induced by pore fluid changes, seafloor roughness, and/or fracturing of the upper-plate (Nishikawa et al., 2019). We note that in the latter case, tremor at seismogenic depths may be viewed as a special case, as it does not fulfill the definition of deep tremor outlined at the beginning of the paper. In addition, we note another unique example involving the subduction of fluid rich sediments, which is also invoked to explain the deep tremor sources (60–80 km) at the eastern termination of the Alaskan Subduction Zone, to date the deepest, well documented example of tremor worldwide (Wech, 2016).

It is unlikely that there are anomalous physical conditions present at the Hellenic and Calabrian subduction zones that would be able to create a deep tremorgenic environment. For instance, heat flow values offshore south of Crete (20–30 mW/m^2; Eckstein, 1978), as well as in continental Calabria (~40 mW/m2; Loddo et al., 1973) are comparatively low and consistent with the age of the subducting slab, hence excluding the presence of a warm, strong megathrust as in the case of Hikurangi (Gao & Wang, 2014). The mantle wedge corner at both subduction zones is expected to be poorly hydrated because of the old nature of the subducting lithosphere (Abers et al., 2017; Halpaap et al., 2019). It is also likely poorly hydrated beneath Crete because the current subduction configuration was reached only 15–20 Ma ago (Thomson et al., 1999). It has been proposed that temperature-dependent silica precipitation by upward migrating fluid derived from the down-going slab reduces permeability in the forearc crust and favors

fluid overpressure, and therefore deep tremorgenic conditions (Audet & Bürgmann, 2014). The potential for silica-rich fluids exists in subduction zones where conditions favor high temperatures (Manning, 1997), and it is greatly enhanced by complete serpentinization of the mantle wedge corner (Audet & Bürgmann, 2014). At both the analyzed subduction zones, such conditions are not met.

The role that the very thick layer of sediments on the down-going plate could play is not easy to address. Deep tremor is observed in erosional (e.g., Mexico) as well as in accretional (e.g., Cascadia or Nankai) subducting margins (Clift & Vannucchi, 2004). Sediments are water rich and can transport it up to 200 km depth (van Keken et al., 2011). However, they release a considerably smaller amount of water than other slab dehydration sources (van Keken et al., 2011), therefore are not expected to significantly contribute to the hydration of the mantle wedge corner.

At the Calabrian Arc, the very low convergence rate may affect the occurrence of tremor, as tremor is not observed elsewhere on fault systems moving slower than 5 mm/yr. We note the convergence rates at the Hellenic Subduction Zone are comparable to those of the slower subduction margins where tremor is observed (e.g., Cascadia, Hikurangi), therefore should not prevent tremor occurrence.

This study does not exclude that tremor could occur above the up-dip limit of the seismogenic zone. The presence of widespread mud volcanos between the backstop and the accretionary wedges of both the Calabrian (Panieri et al., 2013) and Hellenic (Huguen et al., 2001) subduction zones hints at large amounts of fluids released by sediments. High pore fluid pressure could promote tremorgenic conditions up-dip of the seismogenic zone (Saffer & Wallace, 2015). To rule out or confirm the occurrence of shallow tremor, the deployment of dense Ocean Bottom Seismometer networks, as for instance in NE Japan (Nishikawa et al., 2019), would be needed.

Very recently SSEs have been found at the down-dip limit of the seismogenic zone, at depths of 20–40 km beneath western Peloponnese (Mouslopoulou et al., 2020) leaving open the possibility that they occur along other segments of the Hellenic Subduction Zone (Saltogianni et al., 2020). Limitations on publicly available geodetic data may have prevented their detection elsewhere. The duration, location, and the equivalent moment magnitude released are consistent with those of long-term SSEs (i.e., durations from months to years, Obara & Kato, 2016), which are suggested to be manifestation of semi-brittle to viscous behavior (Gao & Wang, 2017), and are not commonly associated with tremor (Husker et al., 2012; Obara, 2011). In contrast, semi-brittle to brittle behavior is invoked to explain ETS episodes (Gao & Wang, 2017). The observations of months-long SSEs at the Hellenic Subduction Zone may suggest that the physical conditions are better suited to long-term SSEs occurrence rather than ETS and would be consistent with a lack of deep triggered tremor.

5.2. Absence of Tremor Along the Kefalonia Transform Fault and North Anatolia Fault in the Sea of Marmara

Of the documented cases of tremor along transform margins, the most well-established examples are along the Parkfield-Cholame segment of the San Andreas Fault (Nadeau & Dolenc, 2005; Peng et al., 2009, Shelly, 2017). The occurrence of tremor in the Parkfield-Cholame area is interpreted to be related to the presence of remnants of partially serpentinized mantle wedge from a former subduction zone (Kirby et al., 2014). The frequency of tremor episodes significantly decreases toward NW (Calaveras) and SE (San Jacinto) along the San Andreas Fault (Gomberg et al., 2008; Peng et al., 2009) enhancing the primary control exerted by the water reservoir beneath the Parkfield-Cholame segment. Although less frequent, deep tremor activity beneath the Alpine Fault in New Zealand is also suggested to be related to the presence of high pore fluid pressures (Baratin et al., 2018; Wech et al., 2012). Along the Kefalonia Transform Fault and the North Anatolian Fault segments in the Sea of Marmara, such a fluid source is possibly missing and/or the conditions required to create high fluid pressures and promote tremorgenesis may not exist. Our results along the North Anatolian Fault are consistent with those of Pfohl et al. (2015) who found no unambiguous evidence for triggered or ambient tremor along the central segment of the North Anatolian Fault. In addition, the transtensional regime in the Sea of Marmara may also not be favorable for tremor occurrence, as most observations of tremor occur along compressive or transform/transpressive margins (Figure 1). While the Kefalonia Transform Fault exhibits transpressional deformation like the Alpine and San Andreas Faults, it shows a different tectonic evolution. For example, it is not located along a former suture zone and it is

much younger, with less accumulated displacement (van Hinsbergen et al., 2006). Furthermore, the seismogenic layer and the Moho depths do not occur at anomalous depths at either the Kefalonia Transform Fault or the Çınarcık segment of the North Anatolian Fault (Sections 2.1 and 2.4) that could hint at significantly high or low temperature gradients.

The absence of triggered tremor in the eastern Marmara Sea agrees with the absence of LFE/tremor activity accompanying the ~50-daylong SSE along the Çınarcık Fault (Martínez-Garzón et al., 2019). The absence of ambient tremor associated with the ~50-daylong SSE could be explained in two different ways: (1) the SSE occurred at shallow depth, consistent with the observation of shallow SSEs along adjacent segments of the North Anatolian Fault (Aslan et al., 2019; Rousset et al., 2016); or (2) the SSE occurred at the down-dip limit of the seismogenic zone, and thereby exhibited a similar behavior to that of long-term SSEs. The occurrence of shallow SSEs along adjacent segments of the North Anatolian Fault would support the shallow origin of the signal.

6. Conclusions

We find no unambiguous evidence for deep triggered tremor at the Hellenic Subduction Zone, beneath Crete, at the Calabrian Subduction Zone, at the Kefalonia Transform Fault, and at the North Anatolian Fault in the eastern Marmara Sea, during the passage of surface waves of 16–18 teleseismic events between 2010 and 2020. Furthermore, we find no unambiguous examples of LFE/tremor activity accompanying the SSE in the eastern Marmara Sea and the two SSEs beneath Peloponnese, along the western segment of the Hellenic Subduction Zone. The station coverage in each of the study areas suggest we would be able to detect tremor episodes formed by LFEs as small as M_w ~1.5–1.9 in all the analyzed regions but Peloponnese, where we would be able to detect LFEs down to M_w ~2.7 ± 0.3, that is, similar to larger events detected in the Cascadia Subduction Zone or Mexico. The absence of triggered tremor, strengthened by the absence of ambient tremor during SSE episodes, suggests the absence of favorable physical conditions for a deep tremorgenic zone in the central-eastern Mediterranean basin. Our results add to the body of evidence supporting that the thermal structure has a significant control on the occurrence of deep tremor in subduction zones. The possible absence of fluid sources that would be able to promote elevated pore fluid pressures at the base of the seismogenic layers at the Kefalonia and North Anatolian transform faults could explain the absence of tremor. In addition, the transtensional regime within the Çınarcık basin, in the eastern Sea of Marmara, may not be favorable to the generation of tremor. The absence of tremor episodes accompanying the SSE along the Çınarcık Fault in the eastern Sea of Marmara suggests that the detected ~50-daylong SSE occurred either at shallow depths in agreement with observations from adjacent segments, or that, if deep, could be classified as long-term SSE. The depth range, duration, and absence of deep tremor during the SSEs along the western segment of the Hellenic Subduction Zone (at least during the 2014–2015 SSE, where the station configuration is denser) is consistent with observations of long-term SSEs elsewhere. The null result presented here indicates that conditions for long-term SSEs, likely a manifestation of semi-brittle to viscous behavior, may be more prevalent compared to the conditions suggested for deep tremor that require a restoration of a brittle or semi-brittle regime at depths where rocks would deform viscously under normal conditions.

Data Availability Statement

Data from HL, HP, HC, HA, HT, IV, MN, GE, KO networks used in this study are freely accessible from EIDA database. Access to the GONAF (Bohnhoff et al., 2017) and PIRES (GFZ Potsdam BU-Kandilli, 2006) networks is granted upon request to Marco Bohnhoff (GFZ).

Acknowledgments
G.M.B. has been funded with Ruhr University of Bochum new faculty startup funds awarded to R.M.H. P.M-G. acknowledges funding from the Helmholtz Young Investigators Group: SAIDAN (VH-NG-1323). We are grateful to the National Observatory of Athens (HL), the University of Patra (HP), the University of Thessaloniki (HT), the University of Athens (HA), the Technological Educational Institute of Crete (HC), the INGV (IV), and to KOERI (KO), GEOFON (GE), and MedNet (MN) technical staff for the installation and maintenance of seismic networks and for publicly sharing data. Thanks to the Turkish Disaster and Emergency Management Presidency (AFAD) in Ankara for providing waveform data from the GONAF observatory. Many thanks to Yajing Liu for her constructive comments on a draft of the manuscript and to Satoshi Ide for having shared the envelope cross-correlation code for ambient tremor detection. Thanks to Marco Roth for useful discussions on code optimization. Thanks to Vasso Saltogianni for the helpful discussion on the recently discovered SSEs beneath Peloponnese (Greece). We are grateful to the Editor (Michael Bostock), the Associate Editor, Calum Chamberlain, and an anonymous reviewer for the constructive comments that helped to improve the initial version of the manuscript. Figures were realized using the Global Mapping Tool (Wessel et al., 2013) and matplotlib (Hunter, 2007). Waveform data processing was performed with Obspy v1.1 (Beyreuther et al., 2010). Open Access funding enabled and organized by ProjektDEAL.

References

Abers, G. A., Van Keken, P. E., & Hacker, B. R. (2017). The cold and relatively dry nature of mantle forearcs in subduction zones. *Nature Geoscience*, *10*, 333–337. https://doi.org/10.1038/ngeo2922

AFAD, Disaster and Emergency Management Presidency (Turkey) (1990). *National Seismic Network of Turkey (AFAD) [Data set]*. International Federation of Digital Seismograph Networks. https://doi.org/10.7914/SN/TU

Aiken, C., Peng, Z., & Chao, K. (2013). Tremors along the Queen Charlotte Margin triggered by large teleseismic earthquakes. *Geophysical Research Letters*, *40*, 829–834. https://doi.org/10.1002/grl.50220

Aki, K., & Richards, P. G. (2002). *Quantitative seismology*. 2nd ed. University Science Books.

Armijo, R., Meyer, B., Navarro, S., King, G., & Barka, A. (2002). Asymmetric slip partitioning in the Sea of Marmara pull-apart: A clue to propagation processes of the north Anatolian Fault? *Terra Nova*, *14*, 80–86. https://doi.org/10.1046/j.1365-3121.2002.00397.x

Aslan, G., Lasserre, C., Cakir, Z., Ergintav, S., Özarpaci, S., Dogan, U., et al. (2019). Shallow creep along the 1999 Izmit earthquake rupture (Turkey) from GPS and high temporal resolution interferometric synthetic aperture radar data (2011–2017). *Journal of Geophysical Research: Solid Earth*, *124*, 2218–2236. https://doi.org/10.1029/2018JB017022

Audet, P., Bostock, M. G., Christensen, N. I., & Peacock, S. M. (2009). Seismic evidence for overpressured subducted oceanic crust and megathrust fault sealing. *Nature*, *457*, 76–78. https://doi.org/10.1038/nature07650

Audet, P., & Bürgmann, R. (2014). Possible control of subduction zone slow-earthquake periodicity by silica enrichment. *Nature*, *510*, 389–392. https://doi.org/10.1038/nature13391

Audet, P., & Kim, Y. H. (2016). Teleseismic constraints on the geological environment of deep episodic slow earthquakes in subduction zone forearcs: A review. *Tectonophysics*, *670*, 1–15. https://doi.org/10.1016/j.tecto.2016.01.005

Aristotle University of Thessaloniki Seismological Network (AUTH) (1981). *Permanent regional seismological Network operated by the Aristotle University of Thessaloniki*. International Federation of Digital Seismograph Networks. https://doi.org/10.7914/SN/HT

Baratin, L. M., Chamberlain, C. J., Townend, J., & Savage, M. K. (2018). Focal mechanisms and inter-event times of low-frequency earthquakes reveal quasi-continuous deformation and triggered slow slip on the deep Alpine Fault. *Earth and Planetary Science Letters*, *484*, 111–123. https://doi.org/10.1016/j.epsl.2017.12.021

Becker, D., & Meier, T. (2010). Seismic slip deficit in the southwestern forearc of the Hellenic subduction zone. *Bulletin of the Seismological Society of America*, *100*, 325–342. https://doi.org/10.1785/0120090156

Beyreuther, M., Barsch, R., Krischer, L., Megies, T., Behr, Y., & Wassermann, J. (2010). ObsPy: A Python toolbox for seismology. *Seismological Research Letters*, *81*(3), 530–533. https://doi.org/10.1785/gssrl.81.3.530

Bocchini, G. M., Brüstle, A., Becker, D., Meier, T., van Keken, P. E., Ruscic, M., et al. (2018). Tearing, segmentation, and backstepping of subduction in the Aegean: New insights from seismicity. *Tectonophysics*, *734–735*, 96–118. https://doi.org/10.1016/j.tecto.2018.04.002

Bockholt, B. M., Langston, C. A., Horton, S., Withers, M., & Deshon, H. R. (2014). Mysterious tremor-like signals seen on the reelfoot fault, Northern Tennessee. *Bulletin Seismological Society of America*, *104*(5), 2194–2205. https://doi.org/10.1785/0120140030

Bohnhoff, M., Dresen, G., Ceken, U., Kadirioglu, F. T., Kartal, R. F., Kilic, T., et al. (2017). GONAF - the borehole geophysical observatory at the north Anatolian Fault in the eastern Sea of Marmara. *Scientific Drilling*, *22*, 19–28. https://doi.org/10.5194/sd-22-19-2017

Bohnhoff, M., Makris, J., Papanikolaou, D., & Stavrakakis, G. (2001). Crustal investigation of the Hellenic subduction zone using wide aperture seismic data. *Tectonophysics*, *343*, 239–262. https://doi.org/10.1016/S0040-1951(01)00264-5

Bohnhoff, M., Martínez-Garzón, P., Bulut, F., Stierle, E., & Ben-Zion, Y. (2016). Maximum earthquake magnitudes along different sections of the North Anatolian fault zone. *Tectonophysics*, *674*, 147–165. https://doi.org/10.1016/j.tecto.2016.02.028

Bostock, M. G., Thomas, A. M., Savard, G., Chuang, L., & Rubin, A. M. (2015). Magnitudes and moment duration scaling of low frequency earthquakes beneath southern Vancouver Island. *Journal of Geophysical Research: Solid Earth*, *120*(9), 6329–6350. https://doi.org/10.1002/2015JB012195

Brown, J. R., Beroza, G. C., Ide, S., Ohta, K., Shelly, D. R., Schwartz, S. Y., et al. (2009). Deep low-frequency earthquakes in tremor localize to the plate interface in multiple subduction zones. *Geophysical Research Letters*, *36*, L19306. https://doi.org/10.1029/2009GL040027

Brown, J. R., Prejean, S. G., Beroza, G. C., Gomberg, J. S., & Haeussler, P. J. (2013). Deep low-frequency earthquakes in tectonic tremor along the Alaska-Aleutian subduction zone. *Journal of Geophysical Research: Solid Earth*, *118*, 1079–1090. https://doi.org/10.1029/2012JB009459

Brudzinski, M. R., Schlanser, K. M., Kelly, N. J., DeMets, C., Grand, S. P., Márquez-Azúa, B., & Cabral-Cano, E. (2016). Tectonic tremor and slow slip along the northwestern section of the Mexico subduction zone. *Earth and Planetary Science Letters*, *454*, 259–271. https://doi.org/10.1016/j.epsl.2016.08.004

Carafa, M. M. C., Kastelic, V., Bird, P., Maesano, F. E., & Valensise, G. (2018). A "Geodetic Gap" in the Calabrian arc: Evidence for a locked subduction megathrust? *Geophysical Research Letters*, *45*, 1794–1804. https://doi.org/10.1002/2017GL076554

Chamberlain, C. J., Hopp, C. J., Boese, C. M., Warren-Smith, E., Chambers, D., Chu, S. X., et al. (2018). EQcorrscan: Repeating and near-repeating earthquake detection and analysis in python. *Seismological Research Letters*, *89*(1), 173–181. https://doi.org/10.1785/0220170151

Chao, K., & Obara, K. (2016). Triggered tectonic tremor in various types of fault systems of Japan following the 2012 Mw8. 6 Sumatra earthquake. *Journal of Geophysical Research: Solid Earth*, *121*(1), 170–187. https://doi.org/10.1002/2015JB012566

Chao, K., Peng, Z., Fabian, A., & Ojha, L. (2012a). Comparisons of triggered tremor in California. *Bulletin of the Seismological Society of America*, *102*(2), 900–908. https://doi.org/10.1785/0120110151

Chao, K., Peng, Z., Gonzalez-Huizar, H., Aiken, C., Enescu, B., Kao, H., et al. (2013). A Global search for triggered tremor following the 2011 Mw 9.0 Tohoku earthquake. *Bulletin of the Seismological Society of America*, *103*(2B), 1551–1571. https://doi.org/10.1785/0120120171

Chao, K., Peng, Z., Wu, C., Tang, C. C., & Lin, C. H. (2012b). Remote triggering of non-volcanic tremor around Taiwan. *Geophysical Journal International*. https://doi.org/10.1111/j.1365-246X.2011.05261.x

Clift, P., & Vannucchi, P. (2004). Controls on tectonic accretion versus erosion in subduction zones: Implications for the origin and recycling of the continental crust. *Reviews of Geophysics*, *42*, RG2001. https://doi.org/10.1029/2003RG000127

Crotwell, H. P., Owens, T. J., & Ritsema, J. (1999). The TauP Toolkit: Flexible seismic travel-time and ray-path utilities. *Seismological Research Letters*, *70*(2), 154–160. https://doi.org/10.1785/gssrl.70.2.154

de Voogd, B., Truffert, C., Chamot-Rooke, N., Huchon, P., Lallemant, S., & Le Pichon, X. (1992). Two-ship deep seismic soundings in the basins of the Eastern Mediterranean Sea (Pasiphae cruise). *Geophysical Journal International*, *109*(3), 536–552. https://doi.org/10.1111/j.1365-246X.1992.tb00116.x

Dickinson, W. R., & Wernicke, B. P. (1997). Reconciliation of San Andreas slip discrepancy by a combination of interior basin and range extension and transrotation near the coast. *Geology*, *25*(7), 663–665. https://doi.org/10.1130/0091-7613(1997)025<0663:ROSASD>2.3.CO;2

Eckstein, Y. (1978). Review of heat flow data from the eastern Mediterranean region. *Pure and Applied Geophysics*, *117*, 150–159.

Faccenna, C., Becker, T. W., Auer, L., Billi, A., Boschi, L., Brun, J. P., et al. (2014). Mantle dynamics in the Mediterranean. *Reviews of Geophysics*, *52*, 283–332. https://doi.org/10.1002/2013RG000444

Faccenna, C., Funiciello, F., Giardini, D., & Lucente, P. (2001). Episodic back-arc extension during restricted mantle convection in the Central Mediterranean. *Earth and Planetary Science Letters*, *187*(1-2), 105–116. https://doi.org/10.1016/S0012-821X(01)00280-1

Farge, G., Shapiro, N. M., & Frank, W. B. (2020). Moment-duration scaling of low-frequency earthquakes in Guerrero, Mexico. *Journal of Geophysical Research: Solid Earth*, *125*, e2019JB019099. https://doi.org/10.1029/2019JB019099

Fletcher, J. B., & McGarr, A. (2011). Moments, magnitudes, and radiated energies of non-volcanic tremor near Cholame, CA, from ground motion spectra at UPSAR. *Geophysical Research Letters*, *38*(16), L16314. https://doi.org/10.1029/2011GL048636

Fry, B., Chao, K., Bannister, S., Peng, Z., & Wallace, L. (2011). Deep tremor in New Zealand triggered by the 2010 Mw8.8 Chile earthquake. *Geophysical Research Letters*, *38*, L15306. https://doi.org/10.1029/2011GL048319
Gao, X., & Wang, K. (2014). Strength of stick-slip and creeping subduction megathrusts from heat flow observations. *Science*, *345*, 1038–1041. https://doi.org/10.1126/science.1255487
Gao, X., & Wang, K. (2017). Rheological separation of the megathrust seismogenic zone and episodic tremor and slip. *Nature*, *543*(7645), 416–419. https://doi.org/10.1038/nature21389
GEOFON Data Centre (1993). *GEOFON seismic network*. Deutsches GeoForschungsZentrum GFZ. https://doi.org/10.14470/TR560404
GFZ Potsdam BU-Kandilli (2006). *Prince islands real-time earthquake monitoring system*. International Federation of Digital Seismograph Networks. Dataset/Seismic Network. https://doi.org/10.7914/SN/PZ
Ghosh, A., Vidale, J. E., Peng, Z., Creager, K. C., & Houston, H. (2009a). Complex nonvolcanic tremor near Parkfield, California, triggered by the great 2004 Sumatra earthquake. *Journal of Geophysical Research*, *114*, B00A15. https://doi.org/10.1029/2008JB006062
Ghosh, A., Vidale, J. E., Sweet, J. R., Creager, K. C., & Wech, A. G. (2009b). Tremor patches in Cascadia revealed by seismic array analysis. *Geophysical Research Letters*, *36*, L17316. https://doi.org/10.1029/2009GL039080
Gomberg, J., Rubinstein, J. L., Peng, Z., Creager, K. C., Vidale, J. E., & Bodin, P. (2008). Widespread Triggering of Nonvolcanic Tremor in California. *Science*, *319*(5860), 173–173. https://doi.org/10.1126/science.1149164
Gosselin, J. M., Audet, P., Estève, C., McLellan, M., Mosher, S. G., & Schaeffer, A. J. (2020). Seismic evidence for megathrust fault-valve behavior during episodic tremor and slip. *Science Advances*, *6*(4), eaay5174. https://doi.org/10.1126/sciadv.aay5174
Granot, R. (2016). Palaeozoic oceanic crust preserved beneath the eastern Mediterranean. *Nature Geoscience*, *9*, 701–705. https://doi.org/10.1038/ngeo2784
Guidoboni, E., & Comastri, A. (2005). *Catalogue of earthquakes and tsunamis in the Mediterranean area from the 11th to the 15th century*. Rome, Italy: Istituto Nazionale di Geofisica e Vulcanologia.
Halpaap, F., Rondenay, S., Perrin, A., Goes, S., Ottemöller, L., Austrheim, H., et al. (2019). Earthquakes track subduction fluids from slab source to mantle wedge sink. *Science Advances*, *5*(4), eaav7369. https://doi.org/10.1126/sciadv.aav7369
Heimann, S., Kriegerowski, M., Isken, M., Cesca, S., Daout, S., Grigoli, F., et al. (2017). *Pyrocko-An open-source seismology toolbox and library. V. 0.3*, Potsdam: GFZ Data Services. https://doi.org/10.5880/GFZ.2.1.2017.001
Horstmann, T., Harrington, R. M., & Cochran, E. S. (2013). Semiautomated tremor detection using a combined cross-correlation and neural network approach. *Journal of Geophysical Research: Solid Earth*, *118*(9), 4827–4846. https://doi.org/10.1002/jgrb.50345
Houston, H. (2015). Low friction and fault weakening revealed by rising sensitivity of tremor to tidal stress. *Nature Geoscience*, *8*, 409–415. https://doi.org/10.1038/ngeo2419
Huguen, C., Mascle, J., Chaumillon, E., Woodside, J. M., Benkhelil, J., Kopf, A., & Volkonskaïa, A. (2001). Deformational styles of the Eastern Mediterranean ridge and surroundings from combined swath mapping and seismic reflection profiling. *Tectonophysics*, *343*, 21–47. https://doi.org/10.1016/S0040-1951(01)00185-8
Hunter, J. D. (2007). Matplotlib: A 2D graphics environment. *Computing in Science & Engineering*, *9*(3), 90–95. https://doi.org/10.1109/MCSE.2007.55
Husker, A. L., Kostoglodov, V., Cruz-Atienza, V. M., Legrand, D., Shapiro, N. M., Payero, J. S., et al. (2012). Temporal variations of non-volcanic tremor (NVT) locations in the Mexican subduction zone: Finding the NVT sweet spot. *Geochemistry, Geophysics, Geosystems*, *13*, Q03011. https://doi.org/10.1029/2011GC003916
Ide, S. (2010). Striations, duration, migration and tidal response in deep tremor. *Nature*, *466*(7304), 356–359. https://doi.org/10.1038/nature09251
Ide, S. (2012). Variety and spatial heterogeneity of tectonic tremor worldwide. *Journal of Geophysical Research*, *117*, B03302. https://doi.org/10.1029/2011JB008840
INGV Seismological Data Centre (2006). *Rete Sismica Nazionale (RSN)*. Italy: Istituto Nazionale di Geofisica e Vulcanologia (INGV). https://doi.org/10.13127/SD/X0FXnH7QfY
ISC International Seismological Centre (2020). *On-line bulletin*. https://doi.org/10.31905/D808B830
Jenkins, J., Stephenson, S. N., Martínez-Garzón, P., Bohnhoff, M., & Nurlu, M. (2020). Crustal thickness variation across the sea of Marmara region, NW Turkey: A reflection of modern and ancient tectonic processes. *Tectonics*, *39*(7), e2019TC005986. https://doi.org/10.1029/2019TC005986
Kennett, B. L. N., & Engdahl, E. R. (1991). Traveltimes for global earthquake location and phase identification. *Geophysical Journal International*, *105*(2), 429–465. https://doi.org/10.1111/j.1365-246X.1991.tb06724.x
Kim, M. J., Schwartz, S. Y., & Bannister, S. (2011). Non-volcanic tremor associated with the March 2010 Gisborne slow slip event at the Hikurangi subduction margin, New Zealand. *Geophysical Research Letters*, *38*(14), L14301. https://doi.org/10.1029/2011GL048400
Kirby, S. H., Wang, K., & Brocher, T. M. (2014). A large mantle water source for the northern San Andreas Fault system: A ghost of subduction past. *Earth Planets and Space*, *66*, 1–18. https://doi.org/10.1186/1880-5981-66-67
Kodaira, S., Iidaka, T., Kato, A., Park, J. O., Iwasaki, T., & Kaneda, Y. (2004). High pore fluid pressure may cause silent slip in the Nankai Trough. *Science*, *304*(5675), 1295–1298. https://doi.org/10.1126/science.1096535
Kopf, A., Mascle, J., & Klaeschen, D. (2003). The Mediterranean Ridge: A mass balance across the fastest growing accretionary complex on Earth. *Journal of Geophysical Research*, *108*(B8), 2372. https://doi.org/10.1029/2001JB000473
KOERI (2001). *International federation of digital seismograph networks*. Bogazici University Kandilli Observatory and Earthquake Research Institute. https://doi.org/10.7914/SN/KO
Lay, T., & Wallace, T. C. (1995). *Modern global seismology*, Academic Press, San Diego, 521 pp.
Le Pichón, X., Şeng Ör, A. M. C., Kende, J., İmren, C., Henry, P., Grail, C., & Karabulut, H. (2016). Propagation of a strike-slip plate boundary within an extensional environment: The westward propagation of the North Anatolian Fault. *Canadian Journal of Earth Sciences*, *53*(11), 1416–1439. https://doi.org/10.1139/cjes-2015-0129
Loddo, M., Mongelli, F., & Roda, C. (1973). Heat flow in Calabria, Italy. *Nature Physics Science*, *244*, 91–92.
Louvari, E., Kiratzi, A. A., & Papazachos, B. C. (1999). The Cephalonia transform fault and its extension to western Lefkada Island (Greece). *Tectonophysics*, *308*, 223–236. https://doi.org/10.1016/S0040-1951(99)00078-5
Maesano, F. E., Tiberti, M. M., & Basili, R. (2017). The Calabrian Arc: Three-dimensional modelling of the subduction interface. *Scientific Reports*, *7*(1), 1–15. https://doi.org/10.1038/s41598-017-09074-8
Malin, P. E., Bohnhoff, M., Blümle, F., Dresen, G., Martínez-Garzón, P., Nurlu, M., et al. (2018). Microearthquakes preceding a M4.2 Earthquake Offshore Istanbul. *Scientific Reports*, *8*(1), 1–11. https://doi.org/10.1038/s41598-018-34563-9
Manning, C. E. (1997). Coupled reaction and flow in subduction zones: Silica metasomatism in the mantle wedge. In: B. Jamtveit & B. W. D. Yardley (Eds.), *Fluid flow and transport in rocks*. Dordrecht: Springer. https://doi.org/10.1007/978-94-009-1533-6_8

Martínez-Garzón, P., Bohnhoff, M., Mencin, D., Kwiatek, G., Dresen, G., Hodgkinson, K., et al. (2019). Slow strain release along the eastern Marmara region offshore Istanbul in conjunction with enhanced local seismic moment release. *Earth and Planetary Science Letters*, *510*, 209–218. https://doi.org/10.1016/j.epsl.2019.01.001

Martínez-Garzón, P., Heidbach, O., & Bohnhoff, M. (2020). Contemporary stress and strain field in the Mediterranean from stress inversion of focal mechanisms and GPS data. *Tectonophysics*, *774*, 228286.

Matthews, K. J., Maloney, K. T., Zahirovic, S., Williams, S. E., Seton, M., & Müller, R. D. (2016). Global plate boundary evolution and kinematics since the late Paleozoic. *Global and Planetary Change*, *146*, 226–250. https://doi.org/10.1016/j.gloplacha.2016.10.002

McClusky, S., Balassanian, S., Barka, A., Demir, C., Ergintav, S., Georgiev, I., et al. (2000). Global Positioning System constraints on plate kinematics and dynamics in the eastern Mediterranean and Caucasus. *Journal of Geophysical Research: Solid Earth*, *105*, 5695–5719. https://doi.org/10.1029/1999JB900351

MedNet Project Partner Institutions (1990). *Mediterranean Very Broadband Seismographic Network (MedNet)*. Istituto Nazionale di Geofisica e Vulcanologia (INGV). https://doi.org/10.13127/SD/fBBBtDtd6q

Meier, T., Becker, D., Endrun, B., Rische, M., Bohnhoff, M., Stöckhert, B., & Harjes, H.-P. (2007). A model for the Hellenic subduction zone in the area of Crete based on seismological investigations. In T. Taymaz, Y. Yilmaz, & Y. Dilek (Eds.), *The geodynamic of the Aegean and Anatolia* (pp. 183–199). Geological Society, London, Special Publications. https://doi.org/10.1144/SP291.9

Meier, T., Rische, M., Endrun, B., Vafidis, A., & Harjes, H.-P. (2004). Seismicity of the Hellenic subduction zone in the area of western and central Crete observed by temporary local seismic networks. *Tectonophysics*, *383*, 149–169. https://doi.org/10.1016/j.tecto.2004.02.004

Miyazawa, M., & Brodsky, E. E. (2008). Deep low-frequency tremor that correlates with passing surface waves. *Journal of Geophysical Research*, *113*, B01307. https://doi.org/10.1029/2006JB004890

Miyazawa, M., Brodsky, E. E., & Mori, J. (2008). Learning from dynamic triggering of low-frequency tremor in subduction zones. *Earth, Planets and Space*, *60*(10), e17–e20. https://doi.org/10.1186/BF03352858

Mouslopoulou, V., Bocchini, G. M., Cesca, S., Saltogianni, V., Bedford, J., Petersen, G., et al. (2020). Earthquake-swarms, slow-slip and fault-interactions at the western-end of the hellenic subduction system precede the M_w 6.9 Zakynthos earthquake, Greece. *Geochemistry, Geophysics, Geosystems*, *21*, e2020GC009243. https://doi.org/10.1029/2020GC009243

Müller, R. D., Sdrolias, M., Gaina, C., & Roest, W. R. (2008). Age, spreading rates, and spreading asymmetry of the world's ocean crust. *Geochemistry, Geophysics, Geosystems*, *9*, Q04006. https://doi.org/10.1029/2007GC001743

Nadeau, R. M., & Dolenc, D. (2005). Nonvolcanic tremors deep beneath the San Andreas Fault. *Science*, *307*(5708), 389. https://doi.org/10.1126/science.1107142

Nishikawa, T., Matsuzawa, T., Ohta, K., Uchida, N., Nishimura, T., & Ide, S. (2019). The slow earthquake spectrum in the Japan Trench illuminated by the S-net seafloor observatories. *Science*, *365*(6455), 808–813. https://doi.org/10.1126/science.aax5618

NOA National Observatory of Athens, I. O. G (1997). *National observatory of Athens seismic network*. International Federation of Digital Seismograph Networks. https://doi.org/10.7914/SN/HL

Norris, R. J., & Cooper, A. F. (2001). Late Quaternary slip rates and slip partitioning on the Alpine Fault, New Zealand. *Journal of Structural Geology*, *23*(2-3), 507–520. https://doi.org/10.1016/S0191-8141(00)00122-X

Obara, K. (2002). Nonvolcanic deep tremor associated with subduction in southwest Japan. *Science*, *296*(5573), 1679–1681. https://doi.org/10.1126/science.1070378

Obara, K. (2011). Characteristics and interactions between non-volcanic tremor and related slow earthquakes in the Nankai subduction zone, southwest Japan. *Journal of Geodynamics*, *52*(3-4), 229–248. https://doi.org/10.1016/j.jog.2011.04.002

Obara, K., & Kato, A. (2016). Connecting slow earthquakes to huge earthquakes. *Science*, *353*(6296), 253–257. https://doi.org/10.1126/science.aaf1512

Panieri, G., Polonia, A., Lucchi, R. G., Zironi, S., Capotondi, L., Negri, A., & Torelli, L. (2013). Mud volcanoes along the inner deformation front of the Calabrian Arc accretionary wedge (Ionian Sea). *Marine Geology*, *336*, 84–98. https://doi.org/10.1016/j.margeo.2012.11.003

Papadimitriou, E., Karakostas, V., Mesimeri, M., Chouliaras, G., & Kourouklas, C. (2017). The Mw6.5 17 November 2015 Lefkada (Greece) earthquake: Structural interpretation by means of the aftershock analysis. *Pure and Applied Geophysics*, *174*(10), 3869–3888. https://doi.org/10.1007/s00024-017-1601-3

Papazachos, B. C., & Papazachou, C. (2003). *The earthquakes of Greece*. Thessaloniki: Ziti Publications.

Peacock, S. M., & Wang, K. (1999). Seismic consequences of warm versus cool subduction metamorphism: Examples from southwest and northeast Japan. *Science*, *80–286*, 937–939. https://doi.org/10.1126/science.286.5441.937

Peng, Z., & Chao, K. (2008). Non-volcanic tremor beneath the central range in Taiwan triggered by the 2001 Mw 7.8 Kunlun earthquake. *Geophysical Journal International*, *175*(2), 825–829. https://doi.org/10.1111/j.1365-246X.2008.03886.x

Peng, Z., & Gomberg, J. (2010). An integrated perspective of the continuum between earthquakes and slow-slip phenomena. *Nature Geoscience*, *3*(9), 599–607. https://doi.org/10.1038/ngeo940

Peng, Z., Gonzalez-Huizar, H., Chao, K., Aiken, C., Moreno, B., & Armstrong, G. (2013). Tectonic tremor beneath Cuba triggered by the Mw 8.8 maule and Mw 9.0 Tohoku-oki earthquakes. *Bulletin of the Seismological Society of America*, *103*(1), 595–600. https://doi.org/10.1785/0120120253

Peng, Z., Vidale, J. E., Wech, A. G., Nadeau, R. M., & Creager, K. C. (2009). Remote triggering of tremor along the San Andreas Fault in central California. *Journal of Geophysical Research*, *114*(B7), B00A06. https://doi.org/10.1029/2008JB006049

Pérouse, E., Chamot-Rooke, N., Rabaute, A., Briole, P., Jouanne, F., Georgiev, I., & Dimitrov, D. (2012). Bridging onshore and offshore present-day kinematics of central and eastern Mediterranean: Implications for crustal dynamics and mantle flow. *Geochemistry, Geophysics, Geosystems*, *13*(9), Q09013. https://doi.org/10.1029/2012GC004289

Pfohl, A., Warren, L. M., Sit, S., & Brudzinski, M. (2015). Search for tectonic tremor on the central north Anatolian fault, Turkey. *Bulletin of the Seismological Society of America*, *105*(3), 1779–1786. https://doi.org/10.1785/0120140312

Rogers, G., & Dragert, H. (2003). Episodic tremor and slip on the Cascadia subduction zone: The chatter of silent slip. *Science*, *300*(5627), 1942–1943. https://doi.org/10.1126/science.1084783

Romanet, P., Bhat, H. S., Jolivet, R., & Madariaga, R. (2018). Fast and slow slip events emerge due to fault geometrical complexity. *Geophysical Research Letters*, *45*(10), 4809–4819. https://doi.org/10.1029/2018GL077579

Romanet, P., & Ide, S. (2019). Ambient tectonic tremors in manawatu, Cape Turnagain, marlborough, and Puysegur, New Zealand. *Earth Planets and Space*, *71*(1), 1–9. https://doi.org/10.1186/s40623-019-1039-1

Rousset, B., Jolivet, R., Simons, M., Lasserre, C., Riel, B., Milillo, P., et al. (2016). An aseismic slip transient on the North Anatolian Fault. *Geophysical Research Letters*, *43*(7), 3254–3262. https://doi.org/10.1002/2016GL068250

Rubinstein, J. L., La Rocca, M., Vidale, J. E., Creager, K. C., & Wech, A. G. (2008). Tidal modulation of nonvolcanic tremor. *Science*, *319*(5860), 186–189. https://doi.org/10.1126/science.1150558

Rubinstein, J. L., Vidale, J. E., Gomberg, J., Bodin, P., Creager, K. C., & Malone, S. D. (2007). Non-volcanic tremor driven by large transient shear stresses. *Nature*. https://doi.org/10.1038/nature06017

Ryan, W. B. F., Carbotte, S. M., Coplan, J. O., O'Hara, S., Melkonian, A., Arko, R., et al. (2009). Global multi-resolution topography synthesis. *Geochemistry, Geophysics and Geosystems*, *10*, Q03014. https://doi.org/10.1029/2008GC002332

Saffer, D. M., & Wallace, L. M. (2015). The frictional, hydrologic, metamorphic and thermal habitat of shallow slow earthquakes. *Nature Geoscience*, *8*(8), 594–600. https://doi.org/10.1038/ngeo2490

Saltogianni, V., Mouslopoulou, V., Oncken, O., Nicol, A., Gianniou, M., & Mertikas, S. (2020). Elastic fault interactions and earthquake-rupture along the southern Hellenic subduction plate-interface zone in Greece. *Geophysical Research Letters*, *47*, e2019GL086604. https://doi.org/10.1029/2019GL086604

Scholz, C. H. (1998). Earthquakes and friction laws. *Nature*, *391*(6662), 37–42. https://doi.org/10.1038/34097

Selvaggi, G., & Chiarabba, C. (1995). Seismicity and P-wave velocity image of the Southern Tyrrhenian subduction zone. *Geophysical Journal International*, *121*(3), 818–826. https://doi.org/10.1111/j.1365-246X.1995.tb06441.x

Şengör, A. M., Tüysüz, O., İmren, C., Sakınç, M., Eyidoğan, H., Görür, N., et al. (2005). The North Anatolian Fault: A new look. *Annual Review of Earth and Planetary Sciences*, *33*, 37–112. https://doi.org/10.1146/annurev.earth.32.101802.120415

Shelly, D. R. (2017). A 15 year catalog of more than 1 million low-frequency earthquakes: Tracking tremor and slip along the deep San Andreas Fault. *Journal of Geophysical Research: Solid Earth*, *122*(5), 3739–3753. https://doi.org/10.1002/2017JB014047

Shelly, D. R., Beroza, G. C., & Ide, S. (2007a). Complex evolution of transient slip derived from precise tremor locations in western Shikoku, Japan. *Geochemistry, Geophysics, Geosystems*, *8*(10), Q10014. https://doi.org/10.1029/2007GC001640

Shelly, D. R., Beroza, G. C., & Ide, S. (2007b). Non-volcanic tremor and low-frequency earthquake swarms. *Nature*, *446*(7133), 305–307. https://doi.org/10.1038/nature05666

Sodoudi, F., Kind, R., Hatzfeld, D., Priestley, K., Hanka, W., Wylegalla, K., et al. (2006). Lithospheric structure of the Aegean obtained from P and S receiver functions. *Journal of Geophysical Research*, *111*. https://doi.org/10.1029/2005JB003932

Speranza, F., Minelli, L., Pignatelli, A., & Chiappini, M. (2012). The Ionian Sea: The oldest in situ ocean fragment of the world?. *Journal of Geophysical Research*, *117*, 1–13. https://doi.org/10.1029/2012JB009475

Stein, R. S., Barka, A. A., & Dieterich, J. H. (1997). Progressive failure on the North Anatolian fault since 1939 by earthquake stress triggering. *Geophysical Journal International*, *128*(3), 594–604. https://doi.org/10.1111/j.1365-246X.1997.tb05321.x

Sun, W. F., Peng, Z., Lin, C. H., & Chao, K. (2015). Detecting deep tectonic tremor in Taiwan with a dense array. *Bulletin of the Seismological Society of America*, *105*(3), 1349–1358. https://doi.org/10.1785/0120140258

Supino, M., Poiata, N., FestaVilotte, G. J. P., Satriano, C., & Obara, K. (2020). Self-similarity of low-frequency earthquakes. *Scientific Reports*, *10*(1), 1–9. https://doi.org/10.1038/s41598-020-63584-6

Syracuse, E. M., van Keken, P. E., Abers, G. A., Suetsugu, D., Bina, C., Inoue, T., et al. (2010). The global range of subduction zone thermal models. *Physics of the Earth and Planetary Interiors*, *183*, 73–90. https://doi.org/10.1016/j.pepi.2010.02.004

TEIC Technological Educational Institute Of Crete. (2006). *Seismological network of Crete*. International Federation of Digital Seismograph Networks. https://doi.org/10.7914/SN/HC

Thomson, S. N., Stöckhert, B., & Brix, M. R. (1999). Miocene high-pressure metamorphic rocks of Crete, Greece: Rapid exhumation by buoyant escape. In U. Ring, G. Lister, S. Willet, & M. Brandon (Eds.), Exhumation processes: Normal faulting, ductile flow, and erosion. Vol. 154 (pp. 87–107) Geological Society, London, Special Publications. http://dx.doi.org/10.1144/GSL.SP.1999.154.01.04

UA University of Athens (2008). *University of Athens, seismological laboratory*. International Federation of Digital Seismograph Networks. https://doi.org/10.7914/SN/HA

UP University of Patras, G. D (2000). *PSLNET, permanent seismic network operated by the University of Patras, Greece*. International Federation of Digital Seismograph Networks. https://doi.org/10.7914/SN/HP

van Hinsbergen, D. J. J., van der Meer, D. G., Zachariasse, W. J., & Meulenkamp, J. E. (2006). Deformation of western Greece during Neogene clockwise rotation and collision with Apulia. *International Journal of Earth Sciences*, *95*, 463–490. https://doi.org/10.1007/s00531-005-0047-5

van Keken, P. E., Hacker, B. R., Syracuse, E. M., & Abers, G. A. (2011). Subduction factory: 4. Depth-dependent flux of H2O from subducting slabs worldwide. *Journal of Geophysical Research*, *116*, B01401. https://doi.org/10.1029/2010JB007922

Vernant, P., Reilinger, R., & McClusky, S. (2014). Geodetic evidence for low coupling on the Hellenic subduction plate interface. *Earth and Planetary Science Letters*, *385*, 122–129. https://doi.org/10.1016/j.epsl.2013.10.018

Walter, J. I., Schwartz, S. Y., Protti, J. M., & Gonzalez, V. (2011). Persistent tremor within the northern Costa Rica seismogenic zone. *Geophysical Research Letters*, *38*, L01307. https://doi.org/10.1029/2010GL045586

Walter, J. I., Schwartz, S. Y., Protti, M., & Gonzalez, V. (2013). The synchronous occurrence of shallow tremor and very low frequency earthquakes offshore of the Nicoya Peninsula, Costa Rica. *Geophysical Research Letters*, *40*, 1517–1522. https://doi.org/10.1002/grl.50213

Warren-Smith, E., Fry, B., Wallace, L., Chon, E., Henrys, S., Sheehan, A., et al. (2019). Episodic stress and fluid pressure cycling in subducting oceanic crust during slow slip. *Nature Geoscience*, *12*(6), 475–481. https://doi.org/10.1038/s41561-019-0367-x

Wech, A. G. (2016). Extending Alaska's plate boundary: Tectonic tremor generated by Yakutat subduction. *Geology*, *44*(7), 587–590. https://doi.org/10.1130/G37817.1

Wech, A. G., Boese, C. M., Stern, T. A., & Townend, J. (2012). Tectonic tremor and deep slow slip on the Alpine Fault. *Geophysical Research Letters*, *39*, L10303. https://doi.org/10.1029/2012GL051751

Wech, A. G., & Creager, K. C. (2008). Automated detection and location of Cascadia tremor. *Geophysical Research Letters*, *35*, L20302. https://doi.org/10.1029/2008GL035458

Wessel, P., Smith, W. H. F., Scharroo, R., Luis, J., & Wobbe, F. (2013). *Generic mapping tools: Improved version released*. Washington. DC: Eos. https://doi.org/10.1002/2013EO450001

Wollin, C., Bohnhoff, M., Martínez-Garzón, P., Küperkoch, L., & Raub, C. (2018). A unified earthquake catalogue for the Sea of Marmara Region, Turkey, based on automatized phase picking and travel-time inversion: Seismotectonic implications. *Tectonophysics*, *474-478*, 416–444. https://doi.org/10.1016/j.tecto.2018.05.020

Yabe, S., Ide, S., & Yoshioka, S. (2014). Along-strike variations in temperature and tectonic tremor activity along the Hikurangi subduction zone, New Zealand. *Earth Planets and Space*, *66*(1), 142. https://doi.org/10.1186/s40623-014-0142-6

Yang, H., & Peng, Z. (2013). Lack of additional triggered tectonic tremor around the Simi Valley and the San Gabriel Mountain in southern California. *Bulletin of the Seismological Society of America*, *103*(6), 3372–3378. https://doi.org/10.1785/0120130117

Zor, E., Özalaybey, S., & Gürbüz, C. (2006). The crustal structure of the eastern Marmara region, Turkey by teleseismic receiver functions. *Geophysical Journal International*, *167*(1), 213–222. https://doi.org/10.1111/j.1365-246X.2006.03042.x

References From the Supporting Information

Dziewonski, A. M., Chou, T. A., & Woodhouse, J. H. (1981). Determination of earthquake source parameters from waveform data for studies of global and regional seismicity. *Journal of Geophysical Research*, *86*(B4), 2825–2852. https://doi.org/10.1029/JB086iB04p02825

Howell, A., Palamartchouk, K., Papanikolaou, X., Paradissis, D., Raptakis, C., Copley, A., et al. (2017). The 2008 Methoni earthquake sequence: The relationship between the earthquake cycle on the subduction interface and coastal uplift in SW Greece. *Geophysical Journal International*, *208*(3), 1592–1610. https://doi.org/10.1093/gji/ggw462

Ide, S., Beroza, G. C., Shelly, D. R., & Uchide, T. (2007). A scaling law for slow earthquakes. *Nature*, *447*(7140), 76–79. https://doi.org/10.1038/nature05780

Karabulut, H., Schmittbuhl, J., Özalaybey, S., Lengliné, O., Kömeç-Mutlu, A., Durand, V., et al. (2011). Evolution of the seismicity in the eastern Marmara Sea a decade before and after the 17 August 1999 Izmit earthquake. *Tectonophysics*, *510*(1-2), 17–27. https://doi.org/10.1016/j.tecto.2011.07.009

Kassaras, I., Kapetanidis, V., & Karakonstantis, A. (2016). On the spatial distribution of seismicity and the 3D tectonic stress field in western Greece. *Physics and Chemistry of the Earth*, *95*, 50–72. https://doi.org/10.1016/j.pce.2016.03.012

Michel, S., Gualandi, A., & Avouac, J.-P. (2019). Similar scaling laws for earthquakes and Cascadia slow-slip events. *Nature, 574*(7779), 522–526. https://doi.org/10.1038/s41586-019-1673-6

Pinar, A., Kuge, K., & Honkura, Y. (2003). Moment tensor inversion of recent small to moderate sized earthquakes: Implications for seismic hazard and active tectonics beneath the sea of Marmara. *Geophysical Journal International*, *153*(1), 133–145. https://doi.org/10.1046/j.1365-246X.2003.01897.x

Tunç, B., Çaka, D., Irmak, T. S., Woith, H., Tunç, S., Bariş, Ş., et al. (2011). The Armutlu Network: An investigation into the seismotectonic setting of Armutlu-Yalova-Gemlik and the surrounding regions. *Annals of Geophysics*, *54*(1), 35–45. https://doi.org/10.4401/ag-4877